© 2021. Published by The Company of Biologists Ltd | Journal of Cell Science (2021) 134, jcs217356. doi:10.1242/jcs.217356

RESEARCH ARTICLE

Extracellular MIF, but not its homologue D-DT, promotes fibroblast motility independently of its receptor complex CD74/CD44

Paweł Szczęśniak[1], Tamara Henke[1], Suada Fröhlich[1], Uwe Plessmann[2], Henning Urlaub[2,3], Lin Leng[4], Richard Bucala[4], Robert Grosse[5], Andreas Meinhardt[1] and Jörg Klug[1,*]

ABSTRACT

Macrophage migration inhibitory factor (MIF) and its homologue D-dopachrome tautomerase (D-DT) are widely expressed pro-inflammatory cytokines with chemokine-like functions that coordinate a wide spectrum of biological activities, such as migration. Here, we biotin-tagged intracellular MIF/D-DT *in vivo* to identify important cytosolic interactors and found a plethora of actin cytoskeleton-associated proteins. Although the receptor complex between CD74 and CD44 (CD74/CD44) is essential for signalling transduction in fibroblasts via extracellular MIF/D-DT, our interactome data suggested direct effects. We, thus, investigated whether MIF/D-DT can modulate cell migration independently of CD74/CD44. To distinguish between receptor- and non-receptor-mediated motility, we used fibroblasts that are either deficient or that express CD74/CD44 proteins, and treated them with recombinant MIF/D-DT. Interestingly, only MIF could stimulate chemokinesis in the presence or absence of CD74/CD44. The pro-migratory effects of MIF depended on lipid raft/caveolae-mediated but not clathrin-mediated endocytosis, on its tautomerase activity and, probably, on its thiol protein oxidoreductase activity. As MIF treatment restrained actin polymerisation *in vitro*, our findings establish a new intracellular role for MIF/D-DT in driving cell motility through modulation of the actin cytoskeleton.

KEY WORDS: Macrophage migration inhibitory factor, MIF, D-dopachrome tautomerase, D-DT, MIF-2, Interactome, Actin cytoskeleton, CD74/CD44, Fibroblast motility, Chemokinesis, Endocytosis

INTRODUCTION

Macrophage migration inhibitory factor (MIF) and its close homologue D-dopachrome tautomerase (DDT, also known as MIF-2 and, hereafter, referred to as D-DT) are pleiotropic cytokines with chemokine-like, endocrine and enzymatic functions (Wang et al., 2016). MIF/D-DT are widely expressed, are secreted by numerous cell types and typically act in an autocrine (Xie et al., 2016) and paracrine manner (Costa-Silva et al., 2015) via cell surface receptors. Cells that are activated by MIF include immune cells, fibroblasts and the endothelium. In immune cells, MIF modulates migration via its non-cognate C-X-C chemokine receptors CXCR2, CXCR4 and CXCR7 that serve as CD74 co-receptors (Bernhagen et al., 2007). Upon binding of MIF to a complex of CXCR2 and CD74, MIF induces chemotaxis as well as the arrest of PBMC-derived monocytes (Bernhagen et al., 2007) and natural killer T cells (Hsieh et al., 2014). B-cell chemotaxis is promoted via CXCR4/CD74, which is followed by Ca^{2+} influx and actin polymerisation (Klasen et al., 2014). Human neutrophils do not express CD74 and, although MIF can bind to CXCR2 alone, MIF exerts only a weak effect on chemotaxis (Bernhagen et al., 2007).

In fibroblasts, MIF binds to CD74 and induces CD44 recruitment, leading to phosphorylation of ERK1 and ERK2 (ERK1/2) that ultimately promotes proliferation and inhibits apoptosis (Shi et al., 2006). MIF also promotes wound healing in NIH 3T3 fibroblasts by inducing calcium influx (Tarnowski et al., 2010), but conversely, inhibits the recruitment of cancer-associated fibroblasts (CAFs) in the rhabdomyosarcoma microenvironment (Tarnowski et al., 2010). Because squamous cell carcinoma cells for example cannot degrade the extracellular matrix, CAFs create tracks for them in an integrin- and protease-dependent manner that support carcinoma cell invasion, rendering CAFs and MIF attractive clinical targets (Gaggioli et al., 2007).

Intracellular non-receptor-based signalling mechanisms are also important for MIF function which became evident when cytoplasmic MIF was shown to interact with and to inhibit the activities of Jun-activation-domain-binding protein 1 (JAB1)/constitutive photomorphogenesis 9 (COP9) signalosome complex subunit 5 (Kleemann et al., 2000a). After this seminal finding other intracellular interacting proteins were identified (Bucala, 2012; Fex Svenningsen et al., 2017). This prompted us to employ a systematic MS-based proteomics screen to find novel cytoplasmic interactors in NIH 3T3 fibroblasts, and we identified the ribosomal protein RPS19 (Filip et al., 2009; Li et al., 2018; Lv et al., 2013) and valosin-containing protein (Cayli et al., 2009) as functionally relevant interactors. After D-DT had been discovered (Merk et al., 2012), we added it to our screen, and aim here at interactors that are shared by MIF and D-DT, which are likely to be important proteins involved in key functions of MIF and D-DT alike.

Intriguingly, we found a very high proportion of actin cytoskeleton-associated proteins that interact with both cytokines. This observation led us to investigate whether the receptors CD74/CD44 are necessary for the modulation of cell motility or whether endocytosed MIF can act in an 'intracrine' manner to modulate cell motility.

[1]Department of Anatomy and Cell Biology, Justus Liebig University, Aulweg 123, Gießen 35392, Germany. [2]Max Planck Institute for Biophysical Chemistry, Bioanalytical Mass Spectrometry Group, Am Fassberg 11, 37077 Göttingen, Germany. [3]Institute for Clinical Chemistry, Research Group 'Bioanalytics', University Medical Center Göttingen, Robert-Koch-Straße 40, 37075 Göttingen, Germany. [4]Department of Internal Medicine, Yale University School of Medicine, New Haven, CT 06520, USA. [5]Institute of Experimental and Clinical Pharmacology and Toxicology, University of Freiburg, Medical Faculty, Albertstraße 25, 79104 Freiburg, Germany.

*Author for correspondence (joerg.klug@anatomie.med.uni-giessen.de)

P.S., 0000-0003-0805-2633; U.P., 0000-0001-5052-0950; H.U., 0000-0003-1837-5233; L.L., 0000-0002-0605-358X; R.B., 0000-0001-5783-5736; R.G., 0000-0002-3380-5273; A.M., 0000-0003-3711-2746; J.K., 0000-0002-8256-7670

Handling Editor: Daniel Billadeau
Received 8 March 2018; Accepted 7 December 2020

Journal of Cell Science (2021) 134, jcs217356. doi:10.1242/jcs.217356

RESULTS

MIF and D-DT are interacting proteins in fibroblasts that regulate the actin cytoskeleton

Here, our aim was to systematically identify intracellular interactors shared by MIF and D-DT, which are likely to indicate important proteins involved in key MIF and D-DT function. To do so, we used NIH 3T3 fibroblasts, which express low-to-no detectable levels of the MIF binding receptor CD74 (Shih and Floyd-Smith, 1995) but do express the signalling component CD44 (Tzircotis et al., 2005, 2006). We tagged endogenously expressed MIF and D-DT at the C-terminus, by using a short sequence that is recognized and biotinylated by the bacterial biotin ligase BirA (de Boer et al., 2003), as described in detail for MIF (Filip et al., 2009). After pulling down biotinylated proteins from stable NIH 3T3 clones that express tagged MIF or D-DT and BirA ligase with streptavidin agarose, we identified individual proteins by mass spectrometry (MS) to produce MIF and D-DT interactomes. Proteomics data are deposited with PRIDE (see Materials and Methods for details).

We identified 647 proteins by using one of the three baits (human and mouse D-DT and rat MIF) that had been absent in the mock control (BirA alone). Of these, only ten proteins interacted with all three baits (Table 1) with eight of them being involved in actin dynamics. The human paralogs of two proteins not involved in actin dynamics, i.e. ribosomal protein L12 (RPL12) and serpin H1 (SERPINH1) have considerable affinity for the BirA tag (crapome.org) and are most likely to be unspecific. We thus went forward with eight potential and mainly new interacting proteins, which indicate that MIF and D-DT are directly involved in actin polymerisation or regulation of the intracellular actin network.

MIF, but not D-DT, enhances fibroblast chemokinesis independently of the CD74/CD44 receptor complex

As the proteomics data indicated that MIF and D-DT regulate the actin network, we hypothesized that MIF and D-DT have a potential role in cellular motility. To confirm this, we performed chemokinesis assays (Wilkinson, 1998) to monitor the speed and frequency of locomotion of COS-7/M6 fibroblasts exposed to the two chemokines. We seeded the fibroblasts at low confluence into medium with low serum content to optimize the ratio between basal and stimulated chemokinesis. After 6 h, we added MIF, MIF mutants, D-DT or endocytosis inhibitors to the cells, and recorded time-lapse videos over 3.5 h at 30-min intervals. We ultimately tracked ∼100 single cells (Fig. 1A), determined their trajectories (Fig. 1B) and calculated their velocities; the obtained data are provided as boxplots (Figs 1–3).

To determine whether the CD74/CD44 receptor complex is required for modulating chemokinesis by MIF and D-DT, COS-7/M6 fibroblasts, which neither express CD74 (Fernandez-Cuesta et al., 2014) nor CD44, were used. By transfecting COS-7/M6 cells with expression constructs for CD74 and CD44, we generated a subline that is stably expressing $CD74^+/CD44^+$ (hereafter referred to as $CD74^+/CD44^+$ cells), as has been described by Shi et al. (2006). After verifying CD74 and CD44 mRNA and protein expression (Figs S1, S2, Table S1), we initially monitored basal chemokinesis in both wild type COS-7/M6 (WT) and the receptor-positive $CD74^+/CD44^+$ cells. We found both types of fibroblast moved with a median velocity of 70–80 nm/min (Fig. 1C,D, and Table S2). EGF served as positive control, increasing chemokinesis 2-fold in WT and 1.4-fold in $CD74^+/CD44^+$ cells.

MIF, but not D-DT, increased the velocity of WT COS-7 cells 1.4-fold, comparable to levels elicited by EGF in the presence of receptors (Fig. 1C). In the presence of the CD74/CD44 receptor complex, D-DT also augmented the velocity albeit to a lesser extent (1.1-fold) than MIF (Fig. 1D). We saw no synergistic effect of MIF and D-DDT on chemokinesis in these cells. In contrast to native proteins, boiled and thus denatured MIF and D-DT lost their ability to increase motility (Fig. 1D). Taken together MIF, but not D-DT, significantly enhances fibroblast chemokinesis independently of the CD74/CD44 receptor complex. We next tested whether key enzymatic activities of MIF are required to stimulate chemokinesis

MIF tautomerase activity and, probably, its thiol protein oxidoreductase activity are both required to stimulate fibroblast chemokinesis

Both D-DT and MIF possess tautomerase activity to catalyse the tautomerisation of a number of (pseudo)substrates (Harris et al., 2019). Although the physiological substrate(s) are unknown, many pro-inflammatory functions of MIF require its tautomerase activity. However, MIF tautomerase activity is ten-times more potent than D-DT, when L-dopachrome methyl ester is used as an assay substrate (Merk et al., 2011) (Fig. S3). After universal methionine aminopeptidases' cleavage of the initiating methionine residue (Varland et al., 2015), the conserved N-terminal proline residue at position (P2) forms the enzymatic basis of tautomerase activity in

Table 1. Shared interactome of MIF and D-DT

Protein	Symbol	Function	Prot. accession	Molecular mass (kDa)
Actin-related protein 2/3 complex subunit 3	ARPC3	Mediates branched actin network formation	Q9JM76	21
Actin-related protein 2/3 complex subunit 4	ARPC4	Mediates branched actin network formation	P59999	20
F-actin-capping protein subunit alpha-1	CAPZA1	α subunit of the barbed-end actin-binding protein that regulates actin filament growth by capping the barbed (growing) end	P47753	33
F-actin-capping protein subunit beta	CAPZB	β subunit of barbed-end actin-binding protein (*see above*)	P47753	34
Destrin	DSTN	Depolymerises actin	Q9R0P5	19
Moesin	MSN	Crosslinks actin cytoskeleton to the plasma membrane	P26041	68
Nucleoside diphosphate kinase B	NME2 (NDPK-B)	Catalyses the transfer of γ-phosphate from nucleoside triphosphates to nucleoside diphosphates	Q01768	17
60S ribosomal protein L12	RPL12	Binds 26S ribosomal RNA within the large ribosomal subunit	P35979	18
Serpin H1	SERPINH1	A serine protease inhibitor and collagen-specific chaperone	P19324	47
Tropomyosin alpha-4 chain	TPM4	Binds to actin filaments in muscle cells (regulating contraction of striated muscle) and non-muscle cells (stabilising cytoskeleton actin filaments)	Q6IRU2	28

Tagged proteins in NIH3T3 cells were biotinylated *in vivo* before streptavidin pulldown, SDS-PAGE and MS analyses. Only mouse proteins that were found to interact with MIF and D-DT are shown. Entries underlain in grey indicate proteins that are known to interact with the BirA-tag (crapome.org).

Journal of Cell Science (2021) 134, jcs217356. doi:10.1242/jcs.217356

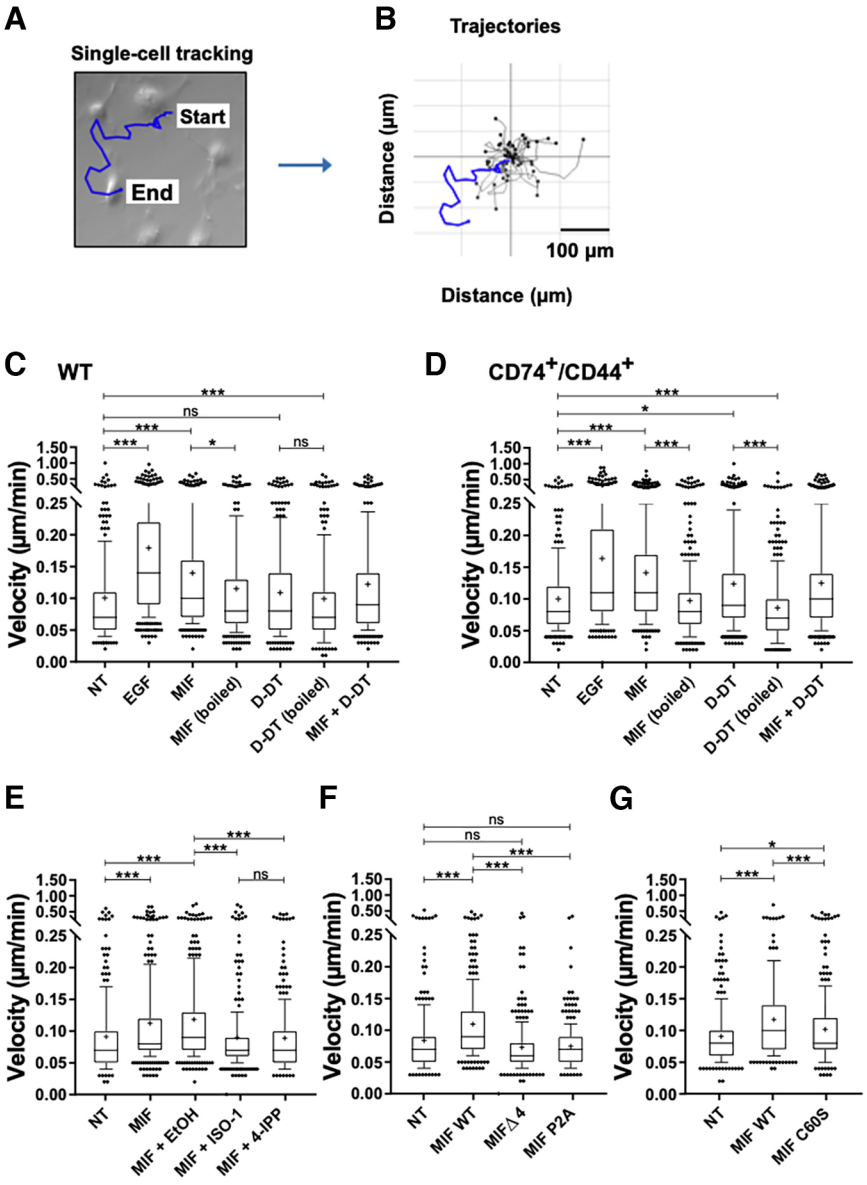

Fig. 1. Exogenous MIF and D-DT upregulate fibroblast chemokinesis dependent on the CD74/CD44 receptor status. MIF residues P2 and C60 are required for enhanced chemokinesis. (A–G) COS-7/M6 cells were seeded and allowed to adhere for 6 h before treatments were performed. Individual cells were tracked in time-lapse videos (A), and trajectories of 100 cells per condition were determined and their velocities calculated (accumulated distance over time in µm/min) (B). WT (C) and $CD74^+/CD44^+$ (D) cells were left untreated (NT), treated with MIF or D-DT (200 ng/ml) that had been denatured (by boiling them) before use or not (all 200 ng/ml), or with MIF plus D-DT. Treatment with EGF (100 ng/ml) was used as a positive control. (E–G) Cells were treated with recombinant MIF (200 ng/ml). This was followed by treatment with MIF tautomerase inhibitors ISO-1 (100 µM) or 4-IPP (50 µM), with ethanol [0.1% (v/v)] as solvent control (EtOH) (E), treatment with the tautomerase-negative MIF-mutants Δ4 and P2A (200 ng/ml each) (F), or treatment with the oxidoreductase-negative mutant MIF C60S (200 ng/ml) (G). Data are shown as boxplots (see Materials and Methods for details). All experiments were performed in triplicates, using cells from three subsequent passages on three different days. Velocity data from three independent wells (replicates) (~300 cells from 30 fields of view) were pooled for each experimental condition. ns, non-significant ($P>0.05$); *$P\leq0.05$; ***$P\leq0.001$.

both proteins. The tautomerase inhibitors 4-IPP (Winner et al., 2008) and ISO-1 (Al-Abed et al., 2005) bind to the catalytic domain and antagonize pro-inflammatory functions of MIF. They also inhibit migration of A549 lung adenocarcinoma cells (Winner et al., 2008) and rhabdomyosarcoma cell lines (Johler et al., 2016). Therefore, we tested whether these inhibitors also affect MIF-driven chemokinesis of WT cells, but not their effects on D-DT, because its chemokinesis and tautomerase activities are much lower. We found that, although MIF alone increased chemokinesis 1.2- or 1.3-fold (Fig. 1A,E) as shown before (Fig. 1A), this effect was abrogated by 4-IPP or ISO-1. We also found no stimulation of chemokinesis when using the tautomerase-null mutants MIF P2A or MIF Δ4, in which the first four amino acids of the N-terminus had been deleted (Filip et al., 2009; Kleemann et al., 2000b) (Fig. 1F).

Next, we investigated whether activity of thiol protein oxidoreductase (TPOR) is required for MIF to stimulate chemokinesis. To do so, we harnessed the TPOR-null mutant that comprises a point mutation of cysteine residue at position 60 to serine (MIF C60S) (Kleemann et al., 1998). Compared to WT MIF, which stimulates chemokinesis 1.3-fold (Fig. 1G), we found that the MIF C60S mutant barely has an effect, as it increases chemokinesis 1.1-fold. These data indicate that MIF tautomerase activity and, probably, also its TPOR activity are crucial to stimulate chemokinesis in WT cells.

Endogenous MIF does not contribute to chemokinesis conferred by exogenous MIF

COS-7/M6 cells express endogenous amounts of MIF that are detectable by western blotting (Fig. 2C, lane 10). We thus wanted to determine whether endogenous MIF contributes to or even promotes the observed effects on chemokinesis. We used two small interfering RNAs (siRNA #1 and #2) and their cognate C911 siRNA as controls (Buehler et al., 2012) to knock down endogenous MIF before exogenous MIF was added to the culture medium. We were able to reduce MIF expression to background levels with each of the two siRNAs in both cell types (Fig. 2C, lanes 2–3 and 5–6) and could almost fully suppress MIF expression when using #1 and #2 siRNAs together (lane 8). We confirmed the specificity of the knock down, as the two C911 siRNA controls did not reduce MIF expression (lanes 4, 7 and 9).

Journal of Cell Science (2021) 134, jcs217356. doi:10.1242/jcs.217356

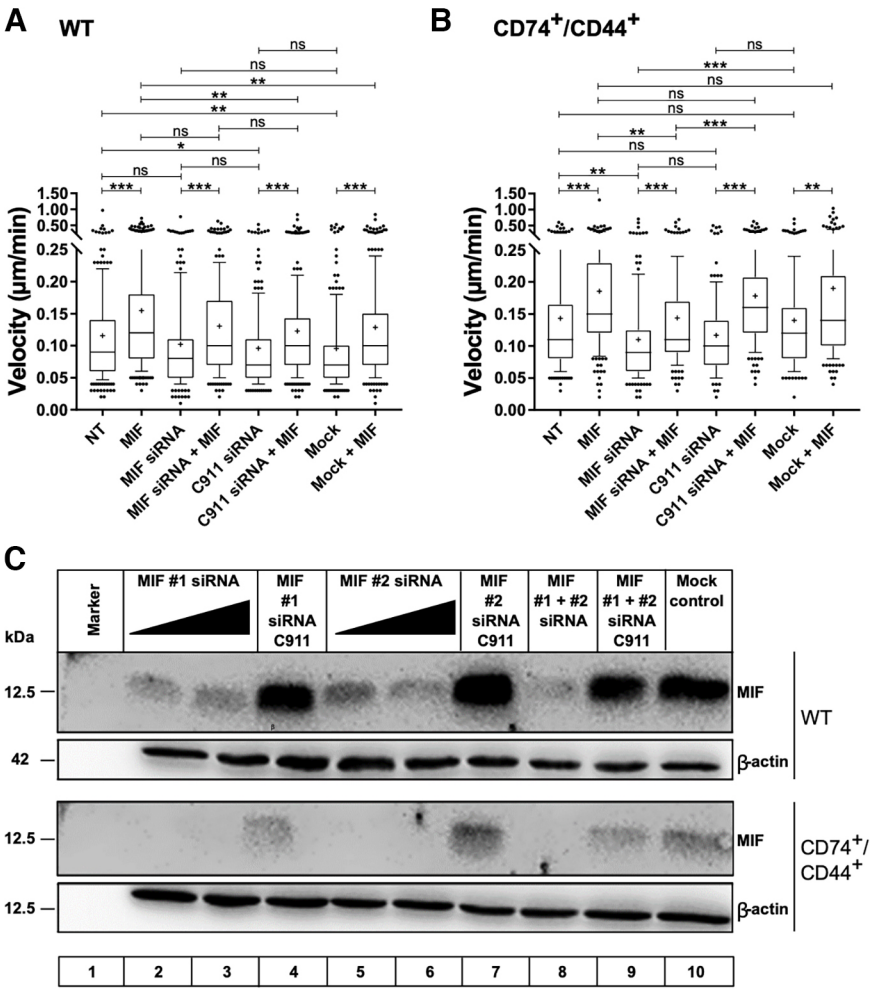

Fig. 2. Endogenous MIF does not contribute to stimulation of chemokinesis in response to exogenous MIF. (A,B) To knock down MIF, WT (A) and CD74$^+$/CD44$^+$ (B) cells were transfected with MIF siRNA #1 and #2 (MIF siRNA), both C911 controls (C911) or transfection reagents only (Mock) and allowed to grow for 2.5 days. Then, cells were seeded in µ-Slides and grown for another 6 h, before MIF addition and cell imaging. (C) Western blot analysis of MIF expression is shown for treated WT (top panel) and CD74$^+$/CD44$^+$ knockdown cells (bottom panel). β-actin was used as loading control. ns, non-significant (P>0.05); *P≤0.05; **P≤0.01; ***P≤0.001.

When MIF was added to the culture medium of WT cells, chemokinesis increased 1.3-fold (Fig. 2A). However, under knockdown conditions, levels of basal chemokinesis dropped to 0.9-fold, which – following addition of exogenous MIF – increased to 1.3-fold (MIF siRNA versus MIF siRNA+MIF) (Fig. 2A). Because both controls, mock and C911, reduced basal chemokinesis to some extent, we concluded this effect to be the result of the transfection procedure. Regardless of the conditions, we were able to enhance chemokinesis with exogenous MIF by 1.3- to 1.4-fold, indicating that the contribution of endogenous MIF is negligible. The results obtained with CD74$^+$/CD44$^+$ cells did not differ qualitatively from those obtained with WT cells (Fig. 2B). We thus conclude that endogenous MIF does not mediate an increase in chemokinesis. Interestingly, we observed that COS-7/M6 WT cells contain ∼80% more endogenous MIF than CD74$^+$/CD44$^+$ cells (Fig. 2C, compare lane 10 in upper and lower MIF panel).

Endocytosis of MIF and D-DT occurs via different pathways to trigger chemokinesis

MIF is endocytosed by several types of cell, including NIH 3T3 fibroblasts (Berndt et al., 2008; Kleemann et al., 2002). To determine which endocytosis pathway does permit exogenous MIF and D-DT to stimulate chemokinesis, we inhibited clathrin-mediated endocytosis (CME) and non-clathrin-mediated endocytosis (non-CME) (Table 2). We used chlorpromazine to inhibit CME, and dynasore to inhibit both CME and a non-CME – the latter inhibits GTPase activity of all three dynamins (Macia et al., 2006) and blocks fluid-phase endocytosis (Park et al., 2013). Chlorpromazine alone had no effect on WT cells but slightly increased basal activity in CD74$^+$/CD44$^+$ cells, whereas dynasore decreased basal activity in both cell lines (Fig. 3A,B and Table 2). When MIF was added to stimulate chemokinesis of WT cells, addition of neither chlorpromazine nor dynasore inhibited this stimulatory effect. This irrespective of whether the effect of MIF was compared with the inhibitor-only control or the non-treated control. However, dynasore, but not chlorpromazine, inhibited MIF-induced chemokinesis of CD74$^+$/CD44$^+$ cells (Fig. 3B), again, irrespective of whether the effect of MIF was compared with the inhibitor-only control or the non-treated control.

Table 2. Effects of CME and non-CME inhibitors on basal levels of chemokinesis or at levels induced by MIF- and D-DT

	WT		CD74$^+$/CD44$^+$		
	∅	MIF	∅	MIF	D-DT
CPZ	→	↑	↑/→	↑	→
DYN	↓	↑/→	↓	→	→
NYS	→	→	→	→	nd
FIL	→	↑/→	→	→	→

Arrows indicate effects of clathrin-mediated endocytosis (CME) or non-CME inhibitors on basal and induced levels of chemokinesis in WT and CD74$^+$/CD44$^+$cells.
∅, basal levels of chemokinesis; MIF, chemokinesis induced by MIF; D-DT, chemokinesis induced by D-DT; nd, not determined; CPZ, chlorpromazine (CME inhibitor); DYN, dynasore (CME and non-CME inhibitor); NYS, nystatin (non-CME inhibitor); FIL, filipin (non-CME inhibitor).

Journal of Cell Science (2021) 134, jcs217356. doi:10.1242/jcs.217356

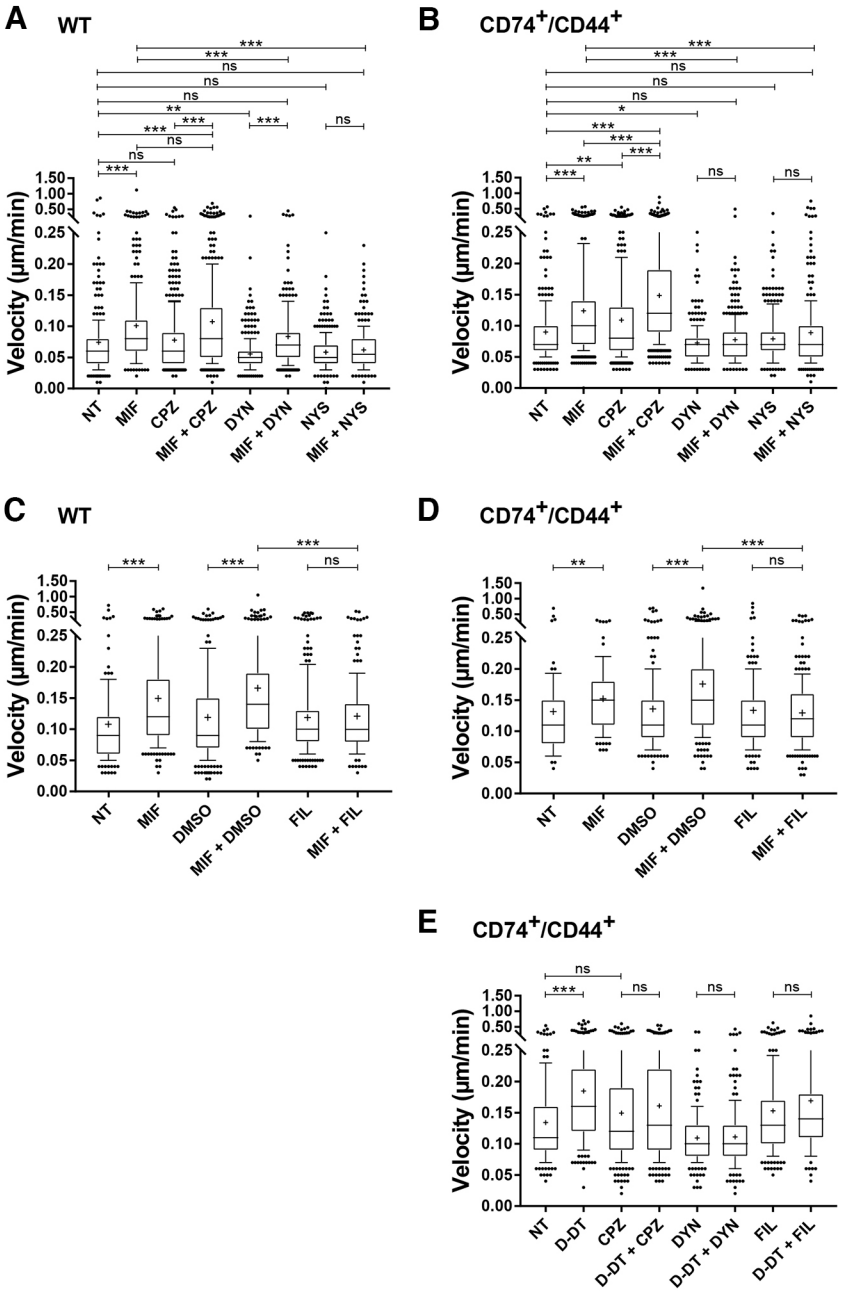

Fig. 3. MIF and D-DT are endocytosed via different pathways to trigger chemokinesis. (A–E) WT (A,C) and CD74$^+$/CD44$^+$ (B,D,E) cells were seeded in µ-Slides and pre-treated with chlorpromazine (CPZ) (10 µM), dynasore (DYN) (50 µM), filipin (FIL) (1.5 µM) or nystatin (NYS) (27 µM) for 1 h before addition of MIF or D-DT (200 ng/ml) and cell imaging. NT, not treated. DMSO [0.02% (v/v)] was used as a solvent control. ns, non-significant (P>0.05); *P≤0.05; **P≤0.01; ***P≤0.001.

We also treated the cells with nystatin, which specifically interferes with lipid raft/caveolae-dependent endocytosis (a part of non-CME) and filipin, which sequesters cholesterol from lipid rafts and also inhibits caveolae-mediated endocytosis (Orlandi and Fishman, 1998). When used alone, neither nystatin nor filipin had an effect on basal chemokinesis, whereas either was able to inhibit MIF-stimulated chemokinesis in both cell lines (Fig. 3C,D). It thus seems that clathrin-coated vesicle formation (Schwartz et al., 2012) is not required for MIF uptake and subsequent chemokinesis. Rather, a lipid raft/caveolae-dependent route is used, where dynamin participates in receptor-positive COS-7/M6 cells only.

We then used the same inhibitors to investigate the D-DT endocytic pathway, but only in CD74$^+$/CD44$^+$ cells, as D-DT did not stimulate chemokinesis in WT cells (Fig. 3E). Again, inhibitors alone had no effect on basal chemokinesis. In contrast to our findings for MIF, chlorpromazine abrogated D-DT-stimulated chemokinesis. Because dynasore and filipin also inhibited D-DT-mediated chemokinesis, we conclude that D-DT is endocytosed via both CME and non-CME pathways.

MIF and D-DT differently affect the rate of actin assembly *in vitro*

Thus far, we found that extracellular MIF and D-DT promote cytokinesis of CD74$^+$/CD44$^+$ cells, and that this effect on migration is dependent on endocytosis. Moreover, most proteins found in the shared interactome of MIF and D-DT are involved in actin dynamics. In our final analyses, we therefore test whether MIF directly or indirectly affects actin assembly. To do so, we established pyrene-labelled actin (pyrene-actin) polymerisation assays, using HEK293 whole cell extract as a source of the actin-related protein 2/3 (ARP2/3) complex (Doolittle et al., 2013). In brief, we activated the polymerisation of fluorescently labelled pyrene-actin by using

Journal of Cell Science (2021) 134, jcs217356. doi:10.1242/jcs.217356

the GST-tagged verprolin, cofilin, acidic (VCA) domain from the Wiskott-Aldrich syndrome protein-family verprolin-homologous protein and measured its emission at 306 nm. The VCA domain was sufficient to induce actin assembly following a logistic curve (Fig. 4). As it is known that the assay conditions are sensitive to small changes in salt concentrations, cognate buffer controls were performed. The buffer control for 1 µm MIF did neither significantly affect polymerisation capacity (i.e. the fluorescence intensity maximum) nor the time at which 50% of polymerisation capacity (T_{50}) was achieved (Fig. 4A and D). However, the buffer control for 3 µm MIF decreased polymerisation capacity by <25% and the T_{50} by 15% (Fig. 4B,D). Compared to these controls, MIF dose dependently slowed down polymerisation velocity as indicated by an increased T_{50} (11% increase with 1 µM MIF and 40% increase with 3 µM MIF) (Fig. 4A,B,D).

The D-DT buffer control had no effect on polymerisation capacity but slowed down velocity by 36% (Fig. 4C,D). Compared to the buffer control, D-DT significantly increased polymerisation velocity to the same extent as buffer alone decreased it. We thus conclude that MIF inhibits the rate of actin polymerisation, whereas D-DT enhances it.

Finally, we repeated this assay in a reconstituted system, by using Arp2/3 purified from pig brain. Here, MIF and D-DT had no significant effect on actin polymerisation (data not shown). Taken together, we conclude that both cytokines do not interact directly with the Arp2/3 complex but require one or more mediating factors that had been provided by the HEK293 cell extract in our assay.

MIF induces F-actin stress fibre formation in COS-7/M6 WT cells

As evidence was pointing to a direct role of MIF in modulating the actin cytoskeleton and, hence, cell motility, the effect of MIF on actin filaments was investigated by using Texas Red X-tagged phalloidin (Fig. 5). Here, the focus was on stress fibre formation, as MIF has previously been implicated in this process (Fan et al., 2011).

For quantification, WT cells were assigned to four categories: (1) cells with prominent stress fibres (Fig. 5A), (2) cells with a prominent cortical actin rim (Fig. 5B), (3) cells with stress fibres and a cortical actin rim (Fig. 5C) and, (4) cells under division. Under starvation conditions (non-treated) <50% of fibroblasts produced a characteristic cortical actin rim around the cell periphery and showed a reduced number of stress fibres (Fig. 5D). Treatment with MIF, but not with heat-inactivated MIF, promoted stress fibre formation – as evidenced by a four-fold increase of the proportion of cells with prominent stress fibres and a 2.5-fold increase compared to non-treated cells (Fig. 5D). Concomitantly, the number of cells with a prominent cortical rim decreased under MIF treatment, whereas the number of dividing cells or of cells positive for both stress fibres and a cortical rim, remained virtually unchanged.

DISCUSSION

Cytokines evolved from intracellular molecules before the appearance of receptors and signalling cascades. Although most cytokines are soluble factors produced by one cell that act on another cell via specific receptors, cytokines can also function as integral membrane proteins or as intracellular proteins that never leave the cell. Although MIF is one of the first cytokines discovered, at a historical perspective it has only been mentioned in recent cytokine reviews (Dinarello, 2007). One reason may be that CD74 (Leng et al., 2003), a type II transmembrane protein, and the non-cognate C-X-C chemokine receptors CXCR2, CXCR4 and CXCR7 that serve as CD74 co-receptors (Bernhagen et al., 2007), were discovered rather late, such that research in the field focussed on receptor signalling mechanisms for many years. We wanted to put intracellular functions of MIF into focus again, aimed at extending previous efforts to identify cytosolic interactors (Cayli et al., 2009; Filip et al., 2009; Lv et al., 2013) by pulling down biotinylated MIF followed by MS-based identification of interacting proteins. We chose NIH 3T3 fibroblasts, which are defective in autocrine MIF signalling as they lack CD74 (Plenker, 2015), and used the paralogous protein D-DT as a second bait to increase the likelihood of finding relevant interactors. Interestingly, eight out of ten newly identified proteins are involved in actin dynamics – most notably two subunits of the ARP2/3 complex and two subunits of capping proteins (Table 1). This finding indicated that MIF and D-DT might regulate migration in a more direct manner than previously thought.

To prove that MIF/D-DT can stimulate migration without involvement of the above mentioned membrane receptors, we

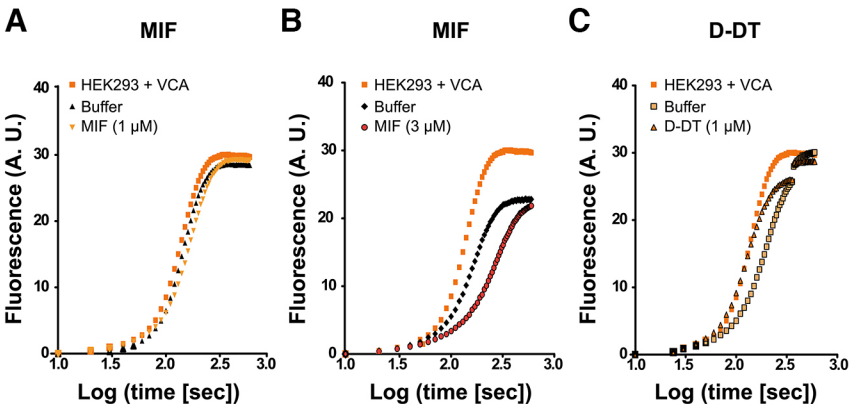

D

	Control	VCA	Buffer M1	MIF (1 µM)	Buffer M3	MIF (3 µM)	Buffer D1	D-DT (1 µM)
T_{50} [s]	478	131	139	158	154	258	205	130
T_{50} [s] 95% CI	451-506	122-142	131-147	146-171	151-156	252-263	189-221	117-145
n	1	3	3	3	3	3	3	3
ANOVA	-	-	-	ns (vs. Buff. M1) ns (vs. VCA)	-	*** (vs. Buff. M3) *** (vs. VCA)	-	* (vs. Buff. D1) ns (vs. VCA)

Fig. 4. Different influence of MIF and D-DT on the rate of actin assembly *in vitro*. (A–C) Non-fluorescent pyrene-labelled G-actin was combined with ARP2/3-containing HEK293 whole cell extract with or without recombinant MIF (A,B) or D-DT (C). The same volume of buffer was used as a control. Formation of filamentous actin was induced using a recombinant VCA domain. Fluorescence of filamentous pyrene-actin was monitored in arbitrary units (A.U.) at 407 nm, with excitation at 365 nm in a 100 µl reaction volume. Original fluorescence traces over time are shown. (D) Data analysis of the pyrene-actin polymerisation assays shown in A–C provided the times when 50% of polymerisation was achieved (T50) and the 95% confidence intervals for T50 (T50 95% c.i.). The numbers of independent samples measured (*n*) and ANOVA results are shown as well. Control treatments (Buffer M1, M3 and D1) simulated the different buffer conditions after treatment with 1 µM MIF (M1), 3 µM MIF (M3) or 1 µM D-DT (D1). ns, non-significant ($P>0.05$); *$P\leq0.01$; ***$P\leq0.001$.

Journal of Cell Science (2021) 134, jcs217356. doi:10.1242/jcs.217356

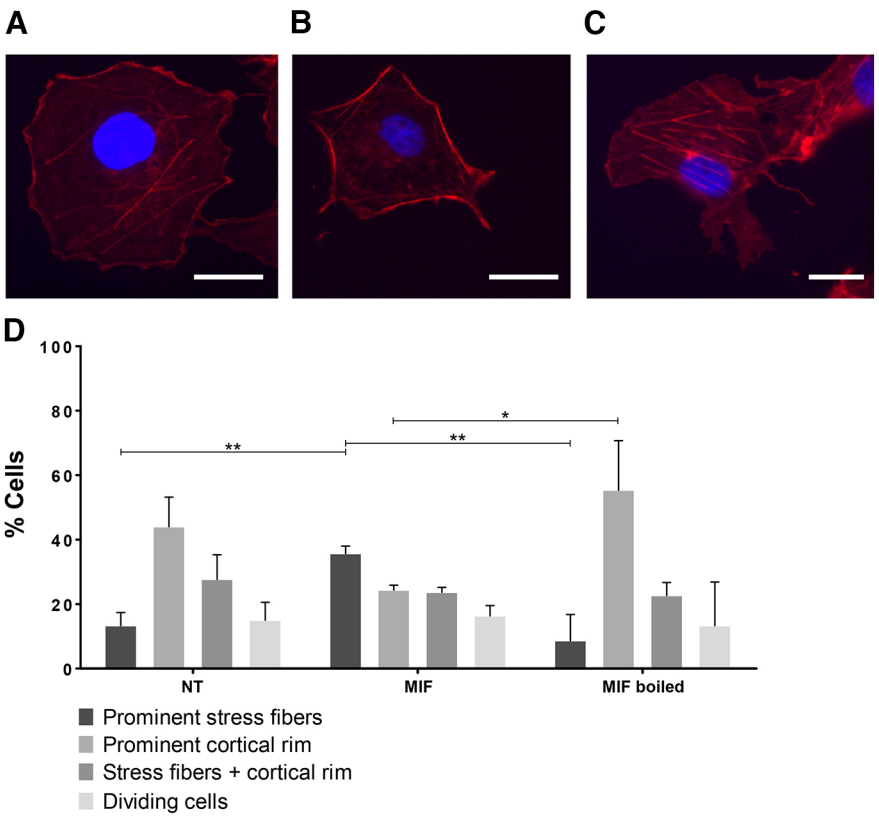

Fig. 5. MIF induces F-actin stress fibre formation in WT cells. WT COS-7/M6 cells were treated for 3.5 h with native or heat-inactivated MIF in medium containing 0.5% (v/v) FCS and stained with Texas-Red conjugated to phalloidin. Cells were mounted with DAPI and visualised using a fluorescence microscope. (A–C) Representative images of cells displaying phalloidin-stained actin. (A) A cell staining positive for both actin stress fibres and a cortical actin rim. (B) A cell showing a prominent cortical actin rim but no or very few stress fibres. (C) A cell showing prominent actin stress fibres but lacking a cortical actin rim. Scale bars: 20 µm. (D) Cells were categorised based on the characteristics of their actin cytoskeleton. Values originate from three independent experiments and represent the mean±s.d. Number of cells used for each treatment assessment: NT, 228; MIF, 436; MIF (boiled), 397. NT, not treated. ANOVA was performed for each category, e.g. prominent stress fibres – a group consisting of NT versus MIF versus MIF (boiled), etc. ns, non-significant (P> 0.05); *P≤0.05; **P≤0.01.

used the mammalian fibroblast-like CD74- and CD44-deficient COS-7/M6 subline, whose cells do not bind MIF unless modified to express CD74 (Leng et al., 2003). These cells had also been used to show that CD44 is the signalling component of the MIF-CD74 receptor complex (Shi et al., 2006). In our subsequent chemokinesis assays, we found that MIF enhanced the motility of CD74/CD44-deficient COS-7/M6 cells to an extent similar to that of receptor-positive $CD74^{+}/CD44^{+}$ cells. By contrast, D-DT could only increase motility in the presence of the CD74/CD44 receptor complex and to a lesser degree than MIF. The potency of MIF, in this respect, is consistent with the higher binding affinity of MIF versus that of D-DT for CD74 (Merk et al., 2011). These results highlight differences between MIF and D-DT (Merk et al., 2012).

We next knocked down intracellular MIF and found no effect on the chemokinesis of receptor-deficient WT cells or of receptor-positive $CD74^{+}/CD44^{+}$ cells in response to extracellular MIF. Previously, similar finding has been obtained for primary mouse embryonic fibroblasts (MEFs), in which short-term exposure to MIF significantly promotes closure of wounded monolayers, regardless whether monolayers were obtained from WT or $MIF^{-/-}$ MEFs (Dewor et al., 2007). Therefore, we conclude that the intracellular pool of MIF does not contribute to induction of cell migration.

The MIF N-terminus includes a catalytic proline residue at position 2 (P2) that is necessary for tautomerase activity. This site has been implicated in mediating MIF function, including the stimulation of cell motility, and provides a target for drugs used to treat several disorders (Al-Abed and VanPatten, 2011; O'Reilly et al., 2016). The deletion of this site renders MIF enzymatically inactive, and prevents interactions between MIF and CD74 , as well as between MIF and intracellular proteins. We found that the tautomerase null mutants MIF P2A and MIF Δ4 do not enhance chemokinesis in WT cells, and that inhibition of tautomerase activity with ISO-1 and 4-IPP abrogated MIF-triggered migration. We thus conclude that the MIF tautomerase activity is required for MIF-mediated fibroblast chemokinesis.

We also found that the oxidoreductase-null MIF C60S mutant increased motility of WT COS-7/M6 cells to a lesser extent than WT MIF; thus, Cys-60 also seems to be important for MIF to upregulate motility. Interestingly, nucleoside diphosphate kinase A (NDPK-A; officially known as NME1) interacts with MIF through the cysteine residue at position 60 and abrogates MIF-induced proliferation of quiescent NIH 3T3 cells and MIF-induced ERK1/2 activation (Jung et al., 2008). Moreover, we found the closely related paralog NME2 (NDPKB) within the shared interactome of MIF and D-DT (Table 1). Because we found that WT MIF decreases the rate of actin assembly only in a cell extract-driven system that should also contain NDPKs, but not in an *in vitro* system with purified components (data not shown), we propose that MIF-induced upregulation of chemokinesis is be mediated by a member of the NDPK family (Fig. 6).

Because MIF upregulates chemokinesis of the CD74/CD44-deficient WT COS-7/M6 cells, but intracellular MIF does not notably contribute to this effect, we concluded that MIF enters the cell to affect cell motility (Fig. 6). Indeed, endocytic uptake of MIF has been demonstrated in many cell types (Berndt et al., 2008). Moreover, it has been found that MIF endocytosis by MEFs and RAW264.7 macrophages seems to be clathrin-mediated (CM) and dependent on CD74 and CXCR4 (Schwartz et al., 2012; Xie et al., 2011). Using chemokinesis as a readout, we found that inhibition of CME with chlorpromazine did not affect MIF-triggered cell motility. We also used dynasore as a cell-permeable inhibitor of both CME and caveolae-mediated endocytosis because both pathways require vesicle scission (von Kleist and Haucke, 2012) that can be inhibited by blocking the GTPase activity of dynamin with dynasore (Ivanov, 2008). From these inhibitor experiments, we found that $CD74^{+}/CD44^{+}$ cells need functional dynamin to

Journal of Cell Science (2021) 134, jcs217356. doi:10.1242/jcs.217356

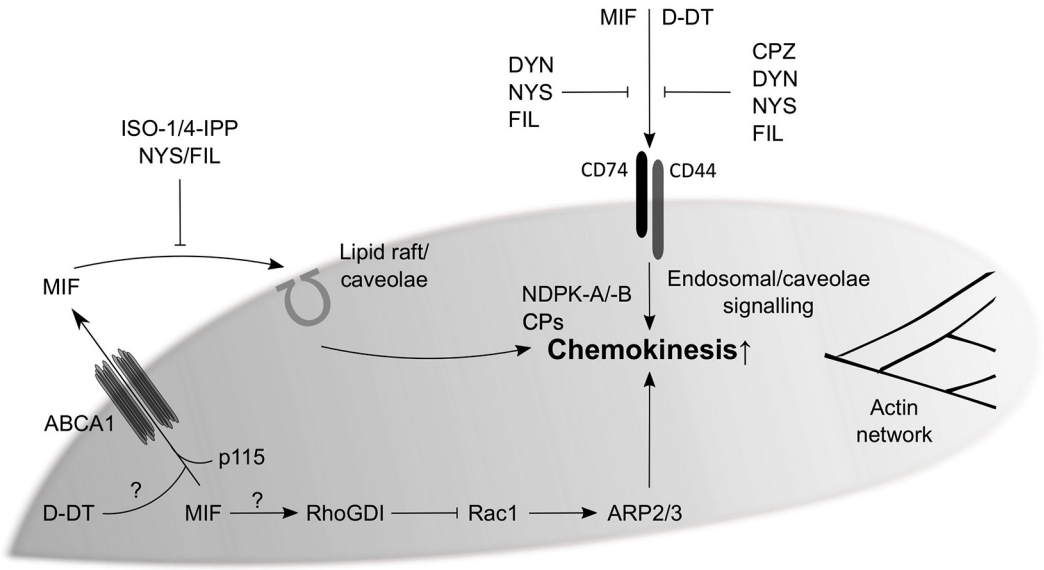

Fig. 6. Extracellular MIF, but not its homologue D-DT, promotes fibroblast motility independently of the CD74/CD44 signalling complex. MIF is secreted via a non-classic pathway, involving the ABCA1 transporter (Flieger et al., 2003). The D-DT secretion route is unknown. Regulated secretion of MIF from monocytes/macrophages is dependent on the Golgi-associated protein p115 (Merk et al., 2009). Once extracellular, MIF – but not D-DT – exerts a chemokinetic effect on receptor-negative WT COS-7/M6 cells, which can be abrogated after treatment with the MIF inhibitors ISO-1 and 4-IPP and the lipid raft/caveolae-mediated endocytosis inhibitors nystatin (NYS) and filipin (FIL). In the presence of the CD74/CD44 signalling complex, MIF and D-DT both engage caveolae-mediated signalling that requires dynamin for vesicle scission. Only D-DT can also engage clathrin-mediated endocytosis and, possibly, endosomal signalling – that might involve nucleoside diphosphate kinase A and B (NDPK-A -B) and capping proteins (CPs). Regulation of chemokinesis by MIF also involves the GTPase Rac1 and, possibly, the Rho GDP-dissociation inhibitor (RhoGDI).

mediate MIF-driven migration, indicating that a non-CME pathway is involved (Fig. 6). These data are consistent with previous findings made in HeLa cells (Schwartz et al., 2012). By contrast, we saw that MIF upregulates motility of WT cells in response to treatment with dynasore, suggesting that MIF is taken up in a non-clathrin and non-dynamin-dependent manner when CD74 and CD44 are absent. Because dynasore can have non-specific effects (Park et al., 2013), we also used two other inhibitors, nystatin and filipin, to disrupt non-CME. Both inhibitors abrogated chemokinesis of WT and $CD74^{+}/CD44^{+}$ cells induced by MIF. From these experiments, we conclude that: (i) dynamin-mediated endocytosis of MIF facilitates MIF-induced upregulation of chemokinesis in CD74- and CD44-positive cells, and, (ii) MIF-mediated chemokinesis is likely to depend on lipid rafts and/or caveolae but not on clathrin or dynamin in CD74- and CD44-negative (receptor-negative) cells.

In line with our results, it has been shown previously that extracellular MIF supports the assembly of caveolin-1-rich lipid raft 'signalling hubs' within the time scale we used for our chemokinesis experiments (Reidy et al., 2013). Moreover, MIF can stabilise the GTPase Rac1 – a master regulator of the actin cytoskeleton and a driver of cell migration – in caveolin-1-rich lipid rafts and, thereby, upregulate the invasiveness of A549 adenocarcinoma cells (Rendon et al., 2007). Interestingly, RhoGDI, a putative MIF interactor, negatively regulates Rac1. MIF overexpression in breast cancer cells also activates caveolin-1 through phosphorylation and promotes cell migration (Lv et al., 2016). Taken together, our findings described here as well as those made by other (Lv et al., 2016; Reidy et al., 2013; Rendon et al., 2007) indicate the existence of an MIF-lipid raft/caveolin signalling cascade that is independent of the classic MIF–CD74/CD44 receptor complex (Fig. 6). Interestingly, Kleemann and colleagues have shown that endocytosis of exogenously added MIF through RAW macrophages is non-saturable over a physiological concentration range and cannot be competed with unlabelled MIF, indicating a receptor-independent pathway (Kleemann et al., 2000a). Differing from MIF, the structural and functional homologue D-DT does require CD74/CD44 to upregulate fibroblast chemokinesis, suggesting that D-DT uses the classic CD74/CD44–Src–ERK1/2 signalling pathway (Shi et al., 2006). However, because our flow cytometry results indicate expression of CXCR4 in COS-7/M6 WT cells, we cannot fully exclude that this receptor is partially contributing to MIF-induced cytokinesis.

In our final analyses, we measured the effects of MIF and D-DT on actin polymerisation in an *in vitro* actin assembly assay, using monomeric pyrene-actin, purified ARP2/3 complex and a recombinant VCA domain as an actin assembly inducer. As we could not detect any change in polymerisation (data not shown), we excluded a direct interaction between MIF and the Arp2/3 complex. We then used a whole cell extract of HEK293 cells as a source for ARP2/3 and ancillary factors, such as NMEs or F-actin or capping proteins (CPs) (Table 1), which might be needed by MIF/D-DT to modulate actin polymerisation. Under these conditions, only MIF but not D-DT dose-dependently restrained the rate of VCA domain-induced actin assembly. Therefore, MIF may function as a CP interactor (Edwards et al., 2014) which can explain restrained actin polymerisation *in vitro* and induced chemokinesis *in vivo*. Moreover, MIF treatment in WT fibroblasts increased the number of stress fibres implicated in cell motility (Taskinen et al., 2020).

Data from this study shed new light on intracellular functions of the cytokine MIF and its close homologue D-DT, elicited by extracellular MIF/D-DT. Therefore, future investigations should focus on further dissecting the internalisation pathway by ablating key endocytosis proteins using Trim-Away (Clift et al., 2017). In addition, studies should directly examine MIF uptake and intracellular tracking, by using, e.g. nanogold labelling. Finally, a more detailed analysis of the changes in actin dynamics and the

exact mechanism(s) MIF/D-DT use to modify the actin cytoskeleton is warranted.

MATERIALS AND METHODS

Inhibitors

Endocytosis inhibitors chlorpromazine (CPZ), filipin III (FIL), nystatin (NYS) and dynasore (DYN) were purchased from Sigma-Aldrich. CPZ was dissolved in water at 50 mM, and FIL at 7.6 mM, NYS at 5.4 mM and DYN at 10 mM all in DMSO. Tautomerase inhibitors (*S,R*)-3-(4-Hydroxyphenyl)-4,5-dihydro-5-isoxazole acetic acid (ISO-1, Merck) and 4-Iodo-6-phenylpyrimidine (4-IPP, Sigma-Aldrich) were dissolved in ethanol at 100 and 50 mM, respectively.

Recombinant proteins

Recombinant human MIF, tautomerase-inactive MIF mutants (MIF Δ4 and MIF P2A) as well as a thiol-protein oxidoreductase-inactive MIF mutant (MIF C60S) were expressed in *E. coli* BL21(DE3) and purified as previously described (Filip et al., 2009). Mouse and human D-DT were also expressed in BL21(DE3) and purified as previously described (Merk et al., 2011). The identity of the recombinant proteins was assessed by matrix assisted laser desorption ionization-time of flight mass spectrometry (MALDI-TOF MS). The protein concentration of the MIF C60S mutant in the supernatant was determined by western blotting, as the protein is prone to precipitating after thawing (Fig. S4). MIF and D-DT heat inactivation was performed at 100°C for 10 min, followed by centrifugation (13,000 ***g***, 15 min) at room temperature.

Cell culture

NIH 3T3 cells (from ATCC) and stable clones thereof were maintained in RPMI 1640 medium. COS-7/M6 fibroblasts (R.B.'s laboratory), stable clones thereof expressing CD74 and CD44 ($CD74^+/CD44^+$ cells), and HEK293 (from ATCC) cells were maintained in DMEM/GlutaMAX high-glucose (4.5 g/l) medium (Life Technologies). All media were supplemented with 10% (v/v) heat-inactivated foetal calf serum, 100 units/ml penicillin and 100 µg/ml streptomycin and incubated at 37°C in a humidified atmosphere with 5% CO_2. All cell lines were regularly tested for mycoplasma contamination by using the group-specific PCR primers GPO-3 (5′-GGGAGCAAACAGGATTAGATACCCT-3′) and MGSO (5′-TGCACCATCTGTCACTCTGTTAACCTC-3′) that amplify a 280-bp fragment in the presence of mycoplasma (van Kuppeveld et al., 1994).

Stable transfection of COS-7/M6 cells

The generation of stable COS-7/M6 cell lines expressing CD44, CD44 Δ67 and/or CD74 has been described elsewhere (Shi et al., 2006). Only CD74/CD44-expressing COS-7/M6 ($CD74^+/CD44^+$) cells were used for this study. They were maintained in the same medium as WT COS-7/M6 cells, but were supplemented with the selection agents zeocin (Invitrogen) and geneticin sulphate (G418) (Calbiochem/Merck) (500 µg/ml each).

Flow cytometry

WT and $CD74^+/CD44^+$ COS-7/M6 cells were washed with PBS, trypsinised, centrifuged for 6 min at 600 ***g***, counted and then washed again with PBS. Then, 2.8×10^6 cells for each group were resuspended in 500 µl PBS/2% FCS, fixed and permeabilised with the Fix & Perm Cell Permeabilization Kit (Thermo Fisher, cat. no. GAS004) according to the manufacturer's protocol. Seven samples comprising 4×10^5 cells each were incubated with 100 µl permeabilization medium and the following antibodies for 30 min: non-stained control (no antibody), 2 µl CD44-APC-H7 (BD, cat. no. 560532), 2 µl CD74-APC (Milteny-Biotec, cat. no. 130-101-543), 1 µl CXCR4-PE (CD184, Milteny-Biotec, cat. no. 130-117-504) and cognate isotype control IgGs (mouse IgG2b, κ APC-H7; BD Pharmingen, cat. no. 560183), mouse IgG1 κ APC (BioLegend cat. no. 130-117-504), recombinant IgG1 PE (Miltenyi-Biotec, cat. no. 130-104-628). The cells were centrifuged for 6 min at 600 ***g*** to remove antibodies, and resuspended in 500 µl PBS/2% FCS before flow cytometry on a BD LSRFortessa (BD Biosciences) using the following channels APC-H7 – R-780/60, PE – G-582/15, and APC – R-670/3. Only live and single cells were analysed. Histograms depicting CD44-, CD74- and CXCR4-positive cell populations were generated using FlowJo (Version 10.5.3) software (BD Biosciences).

Generation of stable NIH 3T3 transfectants expressing biotinylated MIF and D-DT, and identification of interacting proteins

Stable transfection of a gene of interest also encoding a fused 19-amino acid tag that is biotinylated *in vivo* via co-transfected bacterial biotin ligase BirA was achieved as previously described (de Boer et al., 2003). cDNAs encoding rat MIF and human and murine D-DT were subcloned into the modified tagging vector pN3-CTB as described for rat MIF (Filip et al., 2009). NIH 3T3 fibroblasts were stably transfected with linearised pBudCE4.1-birA (de Boer et al., 2003) expressing the biotin ligase and pN3-CTB-rMIF, pN3-CTB-hD-DT (human D-DT) or pN3-CTB-mD-DT (mouse D-DT). Stable clones were isolated and selected for strong expression of MIF and D-DT fusion proteins. NIH 3T3 stable cell lines expressing BirA alone, BirA and MIF, and BirA and D-DT (mouse or human) were maintained in DMEM using 150 µg/ml zeocin (Invitrogen) and/or 100 µg/ml geneticin sulphate (G418) (Calbiochem/Merck) as selection agents. Lysates of all three clones and a control clone expressing BirA only were passed over streptavidin-agarose beads, as described (Filip et al., 2009). After extensive washing, the bound biotinylated protein complexes were eluted by boiling in SDS sample buffer, separated by SDS-PAGE on a 4–12% NuPAGE Bis-Tris gel (Invitrogen) and stained with colloidal Coomassie Blue. All lanes were cut into 12 gel slices, and proteins in all slices were digested with trypsin. Extracted peptides were separated and sequenced by using liquid chromatography (LC) coupled to electrospray ionization (ESI) tandem mass spectrometry (MS/MS) on a quadrupole time of flight (Q-TOF) instrument (Q-TOFUltima, Waters) under standard conditions. Proteins were identified by LC-MS on an Orbitrap XL mass spectrometer (Thermo Fisher Scientific) under standard conditions. Proteins were identified by comparing peptide fragment spectra against mammalian entries in the NCBI database using the MASCOT search engine with standard settings. A Scaffold file, that visualises the proteomics data, is available from J.K. To open a Scaffold file the Scaffold Viewer is required, which is freely available from Proteome Software.

Immunoblot analyses

Cells were lysed in 1% (v/v) IGEPAL® CA-630, 150 mM NaCl, 50 mM Tris-HCl pH 8.0, protease inhibitor cocktail (1:100, Sigma-Aldrich) and 1 mM PMSF. Proteins were separated by SDS-PAGE, and transferred in 25 mM Tris-HCl pH 8.3, 192 mM glycine, 20% (v/v) methanol onto a nitrocellulose membrane using a semi-dry electroblotter (Trans-Blot, Bio-Rad) at 1 mA/cm^2. Membranes were blocked with freshly-made 5% (w/v) non-fat dry milk in TBST [15 mM Tris-HCl pH 7.6, 137 mM NaCl, 1% (v/v) Tween-20] for 1 h. The blocking solution was exchanged for primary antibody-containing milk solution and the membrane was incubated overnight at 4°C with shaking. After washing with TBST, the membranes were incubated at room temperature with shaking in 5% (w/v) non-fat dry milk supplemented with secondary antibodies for 1 h. Primary and secondary antibodies are listed in Table S3.

Membranes were washed with TBST and incubated with ECL substrate {1 ml solution A [0.1 M Tris-HCl pH 8.6, 0.25 mg/ml luminol]; 0.3 µl 30% [v/v] H_2O_2 mixed with 100 µl solution B [1.1 mg/ml p-coumaric acid ((E)-3-(4-hydroxyphenyl)-2-propenoic acid] in DMSO} (Haan and Behrmann, 2007). The ECL signal was detected using a Fusion FX7 imager and analysed with FusionCapt Advance software (Vilber Lourmat, Eberhardzell, Germany).

To re-probe, membranes were incubated in stripping buffer [62 mM Tris-HCl pH 6.8, 0.5% (w/v) SDS, 0.8% (v/v) β-mercaptoethanol] for 5 min at 65°C and washed thoroughly with TBST.

RNA interference

Short interference RNAs (siRNA) were used to deplete endogenous MIF in COS-7/M6 kidney fibroblasts derived from the African green monkey

(*Chlorocebus aethiops*). Human and monkey MIF are virtually identical, with both mRNAs only differing by eight nucleotides within the open reading frame. To knock down human MIF, the sequences of a SMART™ pool were made available by Dharmacon (GE Healthcare) (L-HUMAN-XX-0005). Two sequences were identical to the *Chlorocebus* sequence and selected to knock down the *Chlorocebus* MIF mRNA (Table S4). Cognate C911 controls (Buehler et al., 2012) were used to assess specificity (Table S4).

Lyophilised siRNAs were resuspended in resuspension buffer (60 mM KCl, 6 mM HEPES pH 7.5, 0.2 mM $MgCl_2$) (Dharmacon) to a final concentration of 20 µM. The day before transfection, COS-7/M6 cells were seeded on a 6-well plate at a density of 50,000 cells/well. The next day, the cell culture medium was exchanged for transfection medium comprising 2.5 µl siRNA #1 and/or siRNA #2 (5 µM each) or C911 siRNA controls combined with 15 µl 1× resuspension buffer, and made up to a final volume of 200 µl with Opti-MEM (Gibco). For mock transfections, 200 µl Opti-MEM was used. Separately, 4 µl Lipofectamine™ 2000 Reagent (Invitrogen) was combined with 196 µl Opti-MEM per transfection. After 5 min incubation at room temperature, 200 µl diluted Lipofectamine were added to the siRNA(s) and incubated for an additional 20 min. Then 1.6 ml DMEM/10% (v/v) FCS were added to each transfection. After 6 h, the transfection medium was replaced by DMEM/10% (v/v) FCS without washing. After 3 days of culture, the cells were washed twice with PBS, harvested and lysed for 15 min on ice in lysis buffer [1% (v/v) IGEPAL CA-630, 150 mM NaCl, 50 mM Tris-HCl pH 8.0] containing a protease inhibitor cocktail (Sigma-Aldrich) and 1 mM phenylmethyl sulfonyl fluoride. After centrifugation (13,000 ***g***, 10 min) at 4°C, the supernatant was carefully removed and its protein concentration was determined by Bradford assay (Bradford, 1976).

On the morning of a live-cell imaging experiment (66 h after transfection), cells were dissociated using trypsin, counted, seeded on µ-Slides (ibidi, Martinsried, Germany), and incubated for another 6 h. COS-7/M6 cells (WT and $CD74^+/CD44^+$) were assayed in duplicate on individual µ-Slides and, 72 h after transfection, medium was replaced with medium containing 0.5% (v/v) FCS with or without MIF before acquisition of time-lapse data.

Chemokinesis assays

Cells were seeded at 20% confluence on µ-Slides (13,000 cells per well per cm^2) and allowed to adhere for 6 h to measure cell velocity (velocity=accumulated distance/time in µm/min). For chemokinesis experiments with endocytosis inhibitors, WT and $CD74^+/CD44^+$ COS-7/M6 cells were prepared as described but with the following modifications. The medium was changed from DMEM/10% (v/v) FCS to DMEM/0.5% (v/v) FCS supplemented with endocytosis inhibitors, and the cells were returned to the incubator for 1 h. Without a second medium exchange, MIF was added to the appropriate wells to a final concentration of 200 ng/ml and the cells were imaged for 3.5 h. MIF is found in secretions like saliva, follicular fluid and testicular interstitial fluid in a concentration range up to at least 150 ng/ml. This concentration can be higher under inflammatory conditions. We therefore chose a concentration of 200 ng/ml as it covers the concentration range *in vivo* but does exceed levels that could originate from the secretory activity of the investigated cells. Indeed, 200 ng/ml has also been used in other published analyses (e.g. Klasen et al., 2014).

To set up a time-lapse chemokinesis experiment with COS-7/M6 cells, a live-cell imaging chamber maintaining a humidified atmosphere at 37°C was mounted onto a motorised stage (Nikon Eclipse *Ti* microscope). The NIS-Elements software (Nikon) was initiated and 10 fields of view per treatment were randomly chosen under the 20× objective (200× final magnification; 1 px=0.46 µm). A µ-Slide was carefully mounted in the chamber and data were acquired for at least 3.5 h at 30-min intervals. Following acquisition, the data were exported as image stacks (i.e. video). The cells were selected and their trajectories tracked and saved using the Manual Tracking plug-in of ImageJ (Schneider et al., 2012). The velocities were calculated based on cell trajectories using the Chemotaxis and Migration Tool Ver. 1.01 (ibidi).

Velocity data are represented as boxplots composed of: (*i*) a box (25th–75th percentile); (*ii*) a line in the middle of the box (median) and a plus sign (mean); (*iii*) whiskers (10th–90th percentiles); and (*iv*) dots (outliers; 0th–10th percentile and 90th–100th percentile). In total, ∼100 cells were chosen per condition (one well in a µ-Slide). The final figures present data of ∼300 cells from three single wells in three separate µ-Slides, each representing a different cell passage (n=3), unless otherwise indicated (Kuriyama et al., 2014).

Pyrene-actin polymerisation assays

Pyrene-labelled actin polymerisation assays (Baarlink et al., 2013) were set up by mixing 10 µl energy regenerating mix (150 mM creatine phosphate, 20 mM ATP, 2 mM EGTA, 20 mM $MgCl_2$), 700 µg HEK293 whole cell extract (as an ARP2/3 source), 10 µl GST-tagged VCA domain (1 mg/ml or 2.6 µM) to activate the ARP2/3 complex, 1 µM MIF/D-DT or the same volume of the corresponding buffer, and 10 µl rabbit skeletal muscle α-actin (2 µM final concentration, 10% pyrene-labelled from Hypermol, Bielefeld, Germany) to a final volume of 100 µl with XB buffer (10 mM HEPES pH 7.7, 100 mM KCl, 2 mM $MgCl_2$, 0.1 mM $CaCl_2$, 5 mM EGTA, 1 mM DTT).

HEK293 whole cell extract was prepared as follows. First, the cells were washed twice with PBS and then harvested in the same lysis buffer as WT COS-7/M6 cells. After 15 min incubation on ice, the lysates were centrifuged at 13,000 ***g*** at 4°C for 20 min, and immediately dialysed against XB buffer at 4°C overnight. The final protein concentration was adjusted to ≥10 mg/ml with lysis buffer.

Immediately after the addition of pyrene-actin, the contents of the reaction were mixed by pipetting up and down, and transferred into a black-walled quartz cuvette. Pyrene-actin fluorescence was measured at 10-s intervals for 10 min at 407 nm, with excitation at 365 nm using a RF-5301PC spectrofluorophotometer (Shimadzu, Kyoto, Japan). Data were saved using Panorama Fluorescence software (version 2.1.16.0, Shimadzu/LabCognition Analytical Software, Cologne) and exported as a text file. The fluorescence at time 0 (the first out of 60 measurements is defined as 10 s and the last one as 600 s) was set to zero by subtracting the initial value (in arbitrary units) from all measurements. To calculate the time T_{50} at which 50% pyrene-labelled actin has been polymerised, the function 'log(agonist) vs response - Find ECanything' in GraphPad Prism version 5.04 was used. The default output is the effective concentration (ECF) with the parameter F set to 50.

Actin staining

WT COS-7/M6 cells were seeded at 20,000 cells/cm^2 on round coverslips in a 12-well plate, allowed to adhere overnight and treated with native or heat-inactivated MIF (see above) for 3.5 h. All subsequent steps were performed at room temperature. Cells were fixed with 4% paraformaldehyde (Fluka/Sigma-Aldrich) in PBS for 10 min, washed twice with PBS, permeabilised with 0.1% Triton X-100 (Sigma-Aldrich) in PBS for 3–5 min, washed again twice in PBS, blocked with 1% BSA (Carl Roth) for 30 min and stained with Texas Red-X-conjugated phalloidin (1:500) (Invitrogen) in the dark for 30 min. Following washing, coverslips were removed from the plate, air-dried, overlaid with 4′,6-diamidino-2-phenylindole (DAPI)-containing mounting medium (Vector Laboratories), placed on a glass slide sample side-down and dried overnight in the dark. The next day actin was visualized with an Axioplan 2 imaging microscope (Zeiss) operated with AxioVisio 4.8.2 SP2 software using the excitation/emission wavelengths of 596 nm/615 nm (for Texas Red-X phalloidin) and 358 nm/461 nm (for DAPI). For cell analysis, ImageJ was used to uniformly enhance the contrast in order to better visualise all cytoplasmic actin structures. More than 100 cells were quantified for each sample.

Statistical analyses

GraphPad Prism version 5.04 for Windows (San Diego, CA) was used to perform statistical analyses. For chemokinesis assays, normality of the data was assessed and statistical significance was calculated using a Kruskal–Wallis one-way analysis of variance (ANOVA) with Dunn's multiple comparison test (significance level set to α=0.05) for a group of more than three samples with non-Gaussian distribution (i.e. non-parametric). For actin assembly data analysis, a one-way ANOVA with Tukey's multiple comparison test (significance level set to α=0.05) for a group of three replicates was performed.

Acknowledgements

Bacterial expression clones for MIF mutants were kindly provided by Jürgen Bernhagen (University of Munich, Germany). The authors thank Günter Lochnit (University of Giessen, Germany) for performing additional mass spectrometry,

Margot Zöller (University of Heidelberg, Germany) for the CD44 (Hermes-3) antibody, Jan Faix (MHH Hannover, Germany) and Moritz Winterhoff (TWINCORE, Hannover, Germany) for the *in vitro* actin polymerisation assays, Klaudia Giehl (University of Giessen, Germany) for help with phalloidin stainings, and Jessica Tamanini of Insight Editing London for critical review and editing of the manuscript. The GST-tagged VCA domain was kindly provided by Haicui Wang (R.G.'s lab). Some of the text and figures in this paper formed part of P.S.'s PhD thesis in the Faculties of Veterinary Medicine and Medicine at the Justus Liebig University Giessen in 2016. Intramural funding by the Faculty of Medicine of the Justus-Liebig-Universität Gießen is kindly acknowledged.

Competing interests
The authors declare no competing or financial interests.

Author contributions
Conceptualization: R.B., A.M., J.K.; Formal analysis: P.S.; Investigation: P.S., T.H., S.F., U.P., H.U., L.L.; Resources: U.P., H.U., L.L., R.B., R.G., A.M.; Data curation: P.S., U.P., H.U., J.K.; Writing - original draft: P.S., J.K.; Writing - review & editing: P.S., R.B., A.M., J.K.; Visualization: P.S., J.K.; Supervision: H.U., R.G., A.M., J.K.; Project administration: A.M., J.K.; Funding acquisition: R.G., A.M.

Funding
Intramural funding by the Faculty of Medicine of the Justus-Liebig-Universität Gießen to P.S. is kindly acknowledged.

Data availability
MS proteomics data have been deposited in the ProteomeXchange Consortium via the PRIDE partner repository (Perez-Riverol et al., 2019) and can be accessed with the dataset identifier PXD020449 and DOI 10.6019/PXD020449

Supplementary information
Supplementary information available online at
https://jcs.biologists.org/lookup/doi/10.1242/jcs.217356.supplemental

References
Al-Abed, Y. and VanPatten, S. (2011). MIF as a disease target: ISO-1 as a proof-of-concept therapeutic. *Future Med. Chem.* **3**, 45-63. doi:10.4155/fmc.10.281

Al-Abed, Y., Dabideen, D., Aljabari, B., Valster, A., Messmer, D., Ochani, M., Tanovic, M., Ochani, K., Bacher, M., Nicoletti, F. et al. (2005). ISO-1 binding to the tautomerase active site of MIF inhibits its pro-inflammatory activity and increases survival in severe sepsis. *J. Biol. Chem.* **280**, 36541-36544. doi:10.1074/jbc.C500243200

Baarlink, C., Wang, H. and Grosse, R. (2013). Nuclear actin network assembly by formins regulates the SRF coactivator MAL. *Science* **340**, 864-867. doi:10.1126/science.1235038

Berndt, K., Kim, M., Meinhardt, A. and Klug, J. (2008). Macrophage migration inhibitory factor does not modulate co-activation of androgen receptor by Jab1/CSN5. *Mol. Cell. Biochem.* **307**, 265-271. doi:10.1007/s11010-007-9578-3

Bernhagen, J., Krohn, R., Lue, H., Gregory, J. L., Zernecke, A., Koenen, R. R., Dewor, M., Georgiev, I., Schober, A., Leng, L. et al. (2007). MIF is a noncognate ligand of CXC chemokine receptors in inflammatory and atherogenic cell recruitment. *Nat. Med.* **13**, 587-596. doi:10.1038/nm1567

Bradford, M. M. (1976). A rapid and sensitive method for the quantitation of microgram quantities of protein utilizing the principle of protein-dye binding. *Anal. Biochem.* **72**, 248-254. doi:10.1016/0003-2697(76)90527-3

Bucala, R. (2012). *The MIF Handbook*. Singapore: World Scientific.

Buehler, E., Chen, Y.-C. and Martin, S. (2012). C911: a bench-level control for sequence specific siRNA off-target effects. *PLoS ONE* **7**, e51942. doi:10.1371/journal.pone.0051942

Cayli, S., Klug, J., Chapiro, J., Fröhlich, S., Krasteva, G., Orel, L. and Meinhardt, A. (2009). COP9 signalosome interacts ATP-dependently with p97/valosin-containing protein (VCP) and controls the ubiquitination status of proteins bound to p97/VCP. *J. Biol. Chem.* **284**, 34944-34953. doi:10.1074/jbc.M109.037952

Clift, D., McEwan, W. A., Labzin, L. I., Konieczny, V., Mogessie, B., James, L. C. and Schuh, M. (2017). A method for the acute and rapid degradation of endogenous proteins. *Cell* **171**, 1692-1706.e18. doi:10.1016/j.cell.2017.10.033

Costa-Silva, B., Aiello, N. M., Ocean, A. J., Singh, S., Zhang, H., Thakur, B. K., Becker, A., Hoshino, A., Mark, M. T., Molina, H. et al. (2015). Pancreatic cancer exosomes initiate pre-metastatic niche formation in the liver. *Nat. Cell Biol.* **17**, 816-826. doi:10.1038/ncb3169

de Boer, E., Rodriguez, P., Bonte, E., Krijgsveld, J., Katsantoni, E., Heck, A., Grosveld, F. and Strouboulis, J. (2003). Efficient biotinylation and single-step purification of tagged transcription factors in mammalian cells and transgenic mice. *Proc. Natl. Acad. Sci. USA* **100**, 7480-7485. doi:10.1073/pnas.1332608100

Dewor, M., Steffens, G., Krohn, R., Weber, C., Baron, J. and Bernhagen, J. (2007). Macrophage migration inhibitory factor (MIF) promotes fibroblast migration in scratch-wounded monolayers in vitro. *FEBS Lett.* **581**, 4734-4742. doi:10.1016/j.febslet.2007.08.071

Dinarello, C. A. (2007). Historical insights into cytokines. *Eur. J. Immunol.* **37** Suppl. 1, S34-S45. doi:10.1002/eji.200737772

Doolittle, L. K., Rosen, M. K. and Padrick, S. B. (2013). Measurement and analysis of in vitro actin polymerization. *Methods Mol. Biol.* **1046**, 273-293. doi:10.1007/978-1-62703-538-5_16

Edwards, M., Zwolak, A., Schafer, D. A., Sept, D., Dominguez, R. and Cooper, J. A. (2014). Capping protein regulators fine-tune actin assembly dynamics. *Nat. Rev. Mol. Cell Biol.* **15**, 677-689. doi:10.1038/nrm3869

Fan, H., Hall, P., Santos, L. L., Gregory, J. L., Fingerle-Rowson, G., Bucala, R., Morand, E. F. and Hickey, M. J. (2011). Macrophage migration inhibitory factor and CD74 regulate macrophage chemotactic responses via MAPK and Rho GTPase. *J. Immunol.* **186**, 4915-4924. doi:10.4049/jimmunol.1003713

Fernandez-Cuesta, L., Plenker, D., Osada, H., Sun, R., Menon, R., Leenders, F., Ortiz-Cuaran, S., Peifer, M., Bos, M., Dassler, J. et al. (2014). CD74-NRG1 fusions in lung adenocarcinoma. *Cancer Discov.* **4**, 415-422. doi:10.1158/2159-8290.CD-13-0633

Fex Svenningsen, Å., Löring, S., Sørensen, A. L., Huynh, H. U. B., Hjæresen, S., Martin, N., Moeller, J. B., Elkjær, M. L., Holmskov, U., Illes, Z. et al. (2017). Macrophage migration inhibitory factor (MIF) modulates trophic signaling through interaction with serine protease HTRA1. *Cell. Mol. Life Sci.* **74**, 4561-4572. doi:10.1007/s00018-017-2592-z

Filip, A.-M., Klug, J., Cayli, S., Fröhlich, S., Henke, T., Lacher, P., Eickhoff, R., Bulau, P., Linder, M., Carlsson-Skwirut, C. et al. (2009). Ribosomal protein S19 interacts with macrophage migration inhibitory factor and attenuates its pro-inflammatory function. *J. Biol. Chem.* **284**, 7977-7985. doi:10.1074/jbc.M808620200

Flieger, O., Engling, A., Bucala, R., Lue, H., Nickel, W. and Bernhagen, J. (2003). Regulated secretion of macrophage migration inhibitory factor is mediated by a non-classical pathway involving an ABC transporter. *FEBS Lett.* **551**, 78-86. doi:10.1016/S0014-5793(03)00900-1

Gaggioli, C., Hooper, S., Hidalgo-carcedo, C., Grosse, R. and Marshall, J. F. (2007). Fibroblast-led collective invasion of carcinoma cells with differing roles for RhoGTPases in leading and following cells. *Nat. Cell Biol.* **9**, 1392-1400. doi:10.1038/ncb1658

Haan, C. and Behrmann, I. (2007). A cost effective non-commercial ECL-solution for Western blot detections yielding strong signals and low background. *J. Immunol. Methods* **318**, 11-19. doi:10.1016/j.jim.2006.07.027

Harris, J., VanPatten, S., Deen, N. S., Al-Abed, Y. and Morand, E. F. (2019). Rediscovering MIF: new tricks for an old cytokine. *Trends Immunol.* **40**, 447-462. doi:10.1016/j.it.2019.03.002

Hsieh, C.-Y., Chen, C.-L., Lin, Y.-S., Yeh, T.-M., Tsai, T.-T., Hong, M.-Y. and Lin, C.-F. (2014). Macrophage migration inhibitory factor triggers chemotaxis of $CD74^{+}CXCR2^{+}$ NKT cells in chemically induced IFN-γ-mediated skin inflammation. *J. Immunol.* **193**, 3693-3703. doi:10.4049/jimmunol.1400692

Ivanov, A. I. (2008). Exocytosis and endocytosis. Preface. *Methods Mol. Biol.* **440**, v-vi. doi:10.1007/978-1-59745-178-9

Jiang, H., Peterson, R. S., Wang, W., Bartnik, E., Knudson, C. B. and Knudson, W. (2002). A requirement for the CD44 cytoplasmic domain for hyaluronan binding, pericellular matrix assembly, and receptor-mediated endocytosis in COS-7 cells. *J. Biol. Chem.* **277**, 10531-10538. doi:10.1074/jbc.M108654200

Johler, S. M., Fuchs, J., Seitz, G. and Armeanu-Ebinger, S. (2016). Macrophage migration inhibitory factor (MIF) is induced by cytotoxic drugs and is involved in immune escape and migration in childhood rhabdomyosarcoma. *Cancer Immunol. Immunother.* **65**, 1465-1476. doi:10.1007/s00262-016-1896-4

Jung, H., Seong, H.-A. and Ha, H. (2008). Direct interaction between NM23-H1 and macrophage migration inhibitory factor (MIF) is critical for alleviation of MIF-mediated suppression of p53 activity. *J. Biol. Chem.* **283**, 32669-32679. doi:10.1074/jbc.M806225200

Klasen, C., Ohl, K., Sternkopf, M., Shachar, I., Schmitz, C., Heussen, N., Hobeika, E., Levit-Zerdoun, E., Tenbrock, K., Reth, M. et al. (2014). MIF promotes B cell chemotaxis through the receptors CXCR4 and CD74 and ZAP-70 signaling. *J. Immunol.* **192**, 5273-5284. doi:10.4049/jimmunol.1302209

Kleemann, R., Kapurniotu, A., Frank, R. W., Gessner, A., Mischke, R., Flieger, O., Jüttner, S., Brunner, H. and Bernhagen, J. (1998). Disulfide analysis reveals a role for macrophage migration inhibitory factor (MIF) as thiol-protein oxidoreductase. *J. Mol. Biol.* **280**, 85-102. doi:10.1006/jmbi.1998.1864

Kleemann, R., Hausser, A., Geiger, G., Mischke, R., Burger-Kentischer, A., Flieger, O., Johannes, F. J., Roger, T., Calandra, T., Kapurniotu, A. et al. (2000a). Intracellular action of the cytokine MIF to modulate AP-1 activity and the cell cycle through Jab1. *Nature* **408**, 211-216. doi:10.1038/35041591

Kleemann, R., Rorsman, H., Rosengren, E., Mischke, R., Mai, N. T. and Bernhagen, J. (2000b). Dissection of the enzymatic and immunologic functions of macrophage migration inhibitory factor: full immunologic activity of N-terminally truncated mutants. *Eur. J. Biochem.* **267**, 7183-7192. doi:10.1046/j.1432-1327.2000.01823.x

Kleemann, R., Grell, M., Mischke, R., Zimmermann, G. and Bernhagen, J. (2002). Receptor binding and cellular uptake studies of macrophage migration

inhibitory factor (MIF): use of biologically active labeled MIF derivatives. *J. Interf. Cytokine Res.* **22**, 351-363. doi:10.1089/107999002753675785

Kuriyama, S., Theveneau, E., Benedetto, A., Parsons, M., Tanaka, M., Charras, G., Kabla, A. and Mayor, R. (2014). *In vivo* collective cell migration requires an LPAR2-dependent increase in tissue fluidity. *J. Cell Biol.* **206**, 113-127. doi:10.1083/jcb.201402093

Leng, L., Metz, C. N., Fang, Y., Xu, J., Donnelly, S., Baugh, J., Delohery, T., Chen, Y., Mitchell, R. A. and Bucala, R. (2003). MIF signal transduction initiated by binding to CD74. *J. Exp. Med.* **197**, 1467-1476. doi:10.1084/jem.20030286

Li, J., Tang, Y., Tang, P. M. K., Lv, J., Huang, X.-R., Carlsson-Skwirut, C., Da Costa, L., Aspesi, A., Fröhlich, S., Szczęśniak, P. et al. (2018). Blocking macrophage migration inhibitory factor protects against cisplatin induced acute kidney injury in mice. *Mol. Ther.* **26**, 2523-2532. doi:10.1016/j.ymthe.2018.07.014

Lv, J., Huang, X. R., Klug, J., Fröhlich, S., Lacher, P., Xu, A., Meinhardt, A. and Lan, H. Y. (2013). Ribosomal protein S19 is a novel therapeutic agent in inflammatory kidney disease. *Clin. Sci.* **124**, 627-637. doi:10.1042/CS20120526

Lv, W., Chen, N., Lin, Y., Ma, H., Ruan, Y., Li, Z., Li, X., Pan, X. and Tian, X. (2016). Macrophage migration inhibitory factor promotes breast cancer metastasis via activation of HMGB1/TLR4/NF kappa B axis. *Cancer Lett.* **375**, 245-255. doi:10.1016/j.canlet.2016.02.005

Macia, E., Ehrlich, M., Massol, R., Boucrot, E., Brunner, C. and Kirchhausen, T. (2006). Dynasore, a cell-permeable inhibitor of dynamin. *Dev. Cell* **10**, 839-850. doi:10.1016/j.devcel.2006.04.002

Merk, M., Baugh, J., Zierow, S., Leng, L., Pal, U., Lee, S. J., Ebert, A. D., Mizue, Y., Trent, J. O., Mitchell, R. et al. (2009). The Golgi-associated protein p115 mediates the secretion of macrophage migration inhibitory factor. *J. Immunol.* **182**, 6896-6906. doi:10.4049/jimmunol.0803710

Merk, M., Zierow, S., Leng, L., Das, R., Du, X., Schulte, W., Fan, J., Lue, H., Chen, Y., Xiong, H. et al. (2011). The D-dopachrome tautomerase (DDT) gene product is a cytokine and functional homolog of macrophage migration inhibitory factor (MIF). *Proc. Natl. Acad. Sci. USA* **108**, E577-E585. doi:10.1073/pnas.1102941108

Merk, M., Mitchell, R. A., Endres, S. and Bucala, R. (2012). D-dopachrome tautomerase (D-DT or MIF-2): doubling the MIF cytokine family. *Cytokine* **59**, 10-17. doi:10.1016/j.cyto.2012.03.014

O'Reilly, C., Doroudian, M., Mawhinney, L. and Donnelly, S. C. (2016). Targeting MIF in cancer: therapeutic strategies, current developments, and future opportunities. *Med. Res. Rev.* **36**, 440-460. doi:10.1002/med.21385

Orlandi, P. A. and Fishman, P. H. (1998). Filipin-dependent inhibition of cholera toxin: evidence for toxin internalization and activation through caveolae-like domains. *J. Cell Biol.* **141**, 905-915. doi:10.1083/jcb.141.4.905

Park, R. J., Shen, H., Liu, L., Liu, X., Ferguson, S. M. and De Camilli, P. (2013). Dynamin triple knockout cells reveal off target effects of commonly used dynamin inhibitors. *J. Cell Sci.* **126**, 5305-5312. doi:10.1242/jcs.138578

Perez-Riverol, Y., Csordas, A., Bai, J., Bernal-Llinares, M., Hewapathirana, S., Kundu, D. J., Inuganti, A., Griss, J., Mayer, G., Eisenacher, M. et al. (2019). The PRIDE database and related tools and resources in 2019: improving support for quantification data. *Nucleic Acids Res.* **47**, D442-D450. doi:10.1093/nar/gky1106

Plenker, D. (2015). *Functional Analysis of CD74-NRG1 - A New Recurrent Oncogenic Gene Fusion in Lung Adenocarcinoma*. Cologne: Thesis, University of Cologne.

Reidy, T., Rittenberg, A., Dwyer, M., D'Ortona, S., Pier, G. and Gadjeva, M. (2013). Homotrimeric macrophage migration inhibitory factor (MIF) drives inflammatory responses in the corneal epithelium by promoting caveolin-rich platform assembly in response to infection. *J. Biol. Chem.* **288**, 8269-8278. doi:10.1074/jbc.M112.351064

Rendon, B. E., Roger, T., Teneng, I., Zhao, M., Al-Abed, Y., Calandra, T. and Mitchell, R. A. (2007). Regulation of human lung adenocarcinoma cell migration and invasion by macrophage migration inhibitory factor. *J. Biol. Chem.* **282**, 29910-29918. doi:10.1074/jbc.M704898200

Schneider, C. A., Rasband, W. S. and Eliceiri, K. W. (2012). NIH Image to ImageJ: 25 years of image analysis. *Nat. Methods* **9**, 671-675. doi:10.1038/nmeth.2089

Schwartz, V., Krüttgen, A., Weis, J., Weber, C., Ostendorf, T., Lue, H. and Bernhagen, J. (2012). Role for CD74 and CXCR4 in clathrin-dependent endocytosis of the cytokine MIF. *Eur. J. Cell Biol.* **91**, 435-449. doi:10.1016/j.ejcb.2011.08.006

Shi, X., Leng, L., Wang, T., Wang, W., Du, X., Li, J., McDonald, C., Chen, Z., Murphy, J. W., Lolis, E. et al. (2006). CD44 is the signaling component of the macrophage migration inhibitory factor-CD74 receptor complex. *Immunity* **25**, 595-606. doi:10.1016/j.immuni.2006.08.020

Shih, N.-Y. and Floyd-Smith, G. (1995). Invariant chain (CD74) gene regulation: Enhanced expression associated with activation of protein kinase Cδ in a murine B lymphoma cell line. *Mol. Immunol.* **32**, 643-650. doi:10.1016/0161-5890(95)00029-E

Tarnowski, M., Grymula, K., Liu, R., Tarnowska, J., Drukala, J., Ratajczak, J., Mitchell, R. A., Ratajczak, M. Z. and Kucia, M. (2010). Macrophage migration inhibitory factor is secreted by rhabdomyosarcoma cells, modulates tumor metastasis by binding to CXCR4 and CXCR7 receptors and inhibits recruitment of cancer-associated fibroblasts. *Mol. Cancer Res.* **8**, 1328-1343. doi:10.1158/1541-7786.MCR-10-0288

Taskinen, M. E., Närvä, E., Conway, J. R. W., Hinojosa, L. S., Lilla, S., Mai, A., De Franceschi, N., Elo, L. L., Grosse, R., Zanivan, S. et al. (2020). MASTL promotes cell contractility and motility through kinase-independent signaling. *J. Cell Biol.* **219**, e201906204. doi:10.1083/jcb.201906204

Tzircotis, G., Thorne, R. F. and Isacke, C. M. (2005). Chemotaxis towards hyaluronan is dependent on CD44 expression and modulated by cell type variation in CD44-hyaluronan binding. *J. Cell Sci.* **118**, 5119-5128. doi:10.1242/jcs.02629

Tzircotis, G., Thorne, R. F. and Isacke, C. M. (2006). Directional sensing of a phorbol ester gradient requires CD44 and is regulated by CD44 phosphorylation. *Oncogene* **25**, 7401-7410. doi:10.1038/sj.onc.1209724

van Kuppeveld, F. J., Johansson, K. E., Galama, J. M., Kissing, J., Bölske, G., van der Logt, J. T. and Melchers, W. J. (1994). Detection of mycoplasma contamination in cell cultures by a mycoplasma group-specific PCR. *Appl. Environ. Microbiol.* **60**, 149-152. doi:10.1128/AEM.60.1.149-152.1994

Varland, S., Osberg, C. and Arnesen, T. (2015). N-terminal modifications of cellular proteins: the enzymes involved, their substrate specificities and biological effects. *Proteomics* **15**, 2385-2401. doi:10.1002/pmic.201400619

von Kleist, L. and Haucke, V. (2012). At the crossroads of chemistry and cell biology: inhibiting membrane traffic by small molecules. *Traffic* **13**, 495-504. doi:10.1111/j.1600-0854.2011.01292.x

Wang, Y., An, R., Umanah, G. K., Park, H., Nambiar, K., Eacker, S. M., Kim, B., Bao, L., Harraz, M. M., Chang, C. et al. (2016). A nuclease that mediates cell death induced by DNA damage and poly(ADP-ribose) polymerase-1. *Science* **354**, aad6872. doi:10.1126/science.aad6872

Wilkinson, P. C. (1998). Assays of leukocyte locomotion and chemotaxis. *J. Immunol. Methods* **216**, 139-153. doi:10.1016/S0022-1759(98)00075-1

Winner, M., Meier, J., Zierow, S., Rendon, B. E., Crichlow, G. V., Riggs, R., Bucala, R., Leng, L., Smith, N., Lolis, E. et al. (2008). A novel, macrophage migration inhibitory factor suicide substrate inhibits motility and growth of lung cancer cells. *Cancer Res.* **68**, 7253-7257. doi:10.1158/0008-5472.CAN-07-6227

Xie, L., Qiao, X., Wu, Y. and Tang, J. (2011). β-Arrestin1 mediates the endocytosis and functions of macrophage migration inhibitory factor. *PLoS ONE* **6**, e16428. doi:10.1371/journal.pone.0016428

Xie, J., Yang, L., Tian, L., Li, W., Yang, L. and Li, L. (2016). Macrophage migration inhibitor factor upregulates MCP-1 expression in an autocrine manner in hepatocytes during acute mouse liver injury. *Sci. Rep.* **6**, 27665. doi:10.1038/srep27665

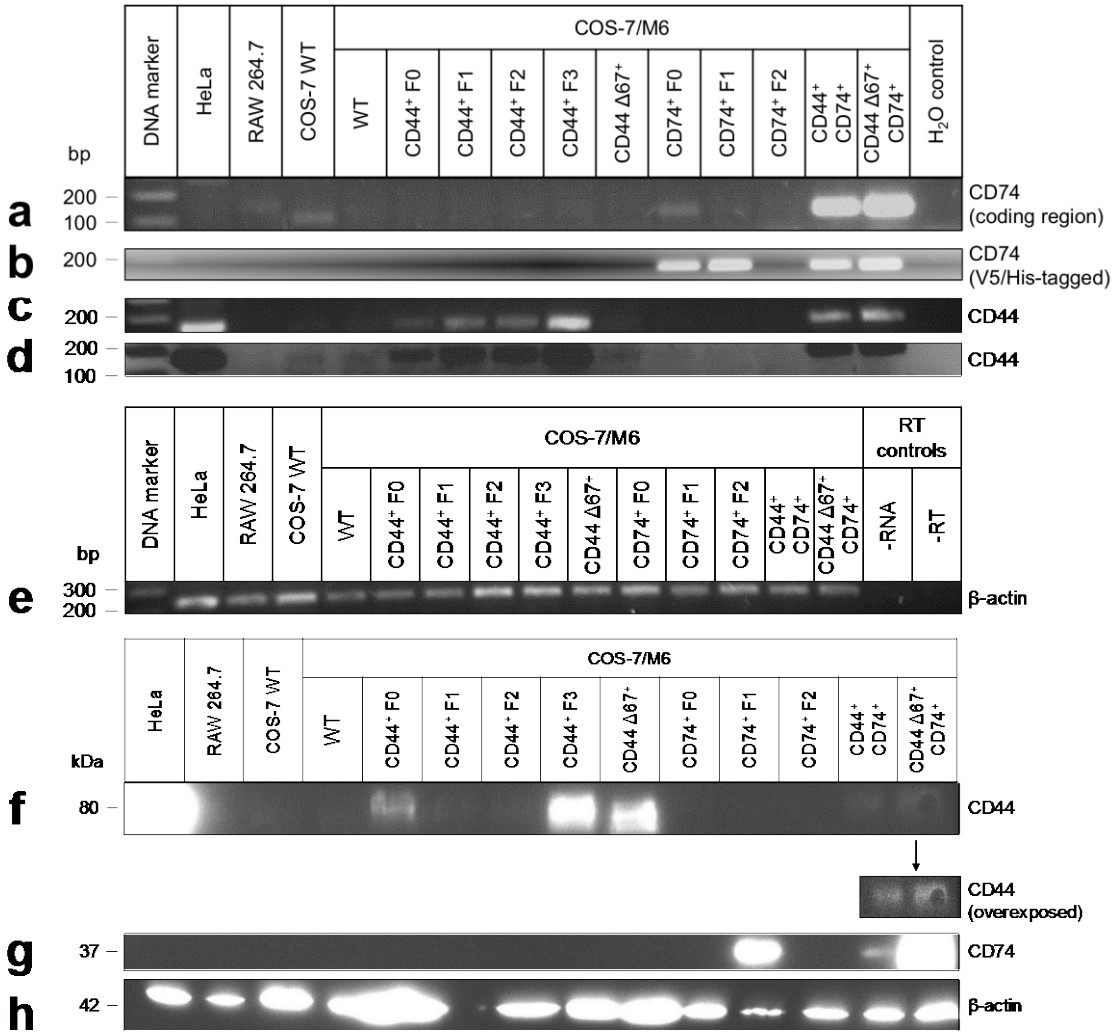

Figure S1. PCR and immunoblot analyses of stable COS-7/M6 cell lines expressing MIF receptors CD74/CD44. (**a-d**) Total RNA from COS-7/M6 cell lines stably transfected with mammalian expression constructs for CD74 and/or CD44 was isolated and reverse-transcribed. Specific gene fragments were amplified using primer pairs as listed in Table S1. PCR samples were resolved on 1.2% agarose gels and stained with ethidium bromide. Note that COS-7 cells are from the African green monkey, and transfected CD74 and CD44 sequences are from man. The figure comprises more cell lines than used in this study. HeLa mRNA was used as a positive control for CD44.

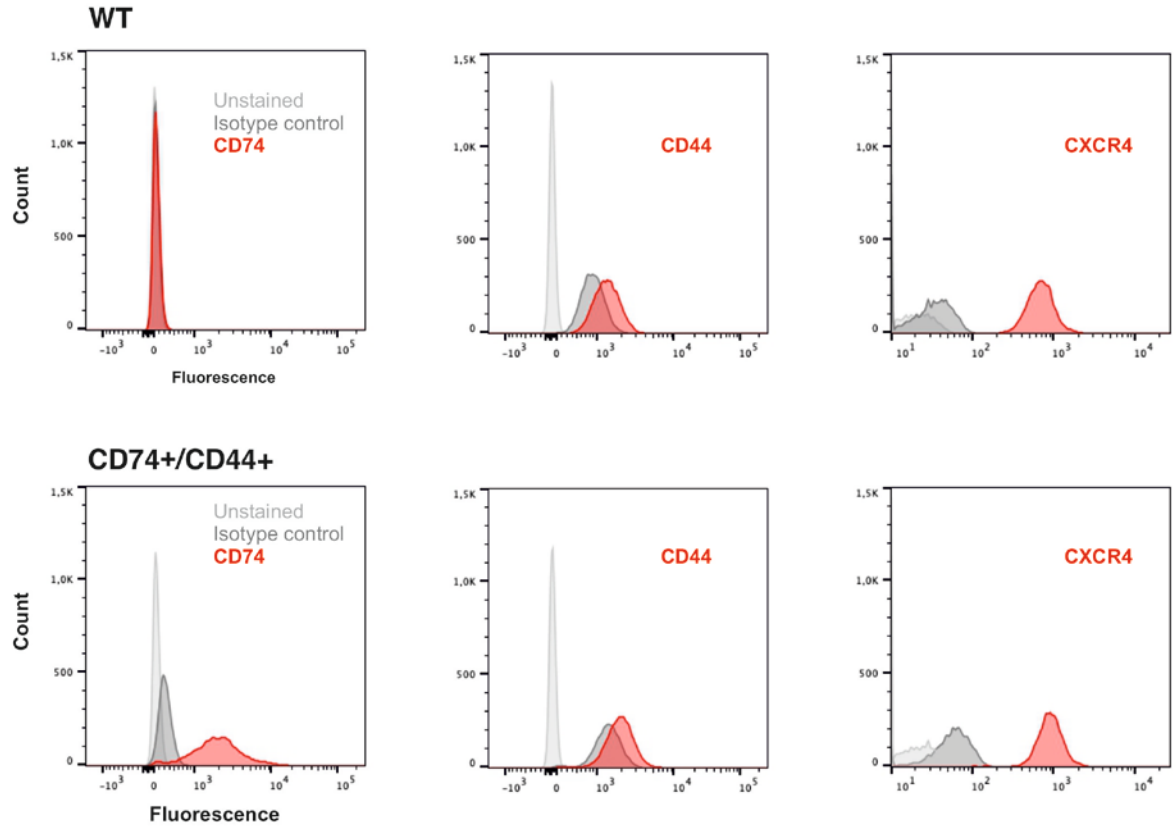

Figure S2. Flow cytometric analyses of WT COS-7/M6 cells (WT) and CD74$^+$/CD44$^+$ COS-7/M6 cells
(CD74+/CD44+) stably transfected with mammalian expression constructs for CD74 and CD44. Cells were fixed, permeabilized and aliquots stained with no antibody (unstained), CXCR4, CD74 or CD44 antibodies or the cognate isotype control antibodies (see Materials and Methods for details). Histograms depicting CD44-, CD74- and CXCR4-positive live and single cell populations were generated using FlowJo (Version 10.5.3) software (BD Biosciences). Both COS-7/M6 cell lines, WT and CD74$^+$/CD44$^+$, are positive for CXCR4. WT cells are negative for CD74 and CD74$^+$/CD44$^+$ cells stain positive. The isotype control for the CD44 antibody used is unspecifically staining WT cells and CD74$^+$CD44$^+$ cells so that the antibody used is not informative.

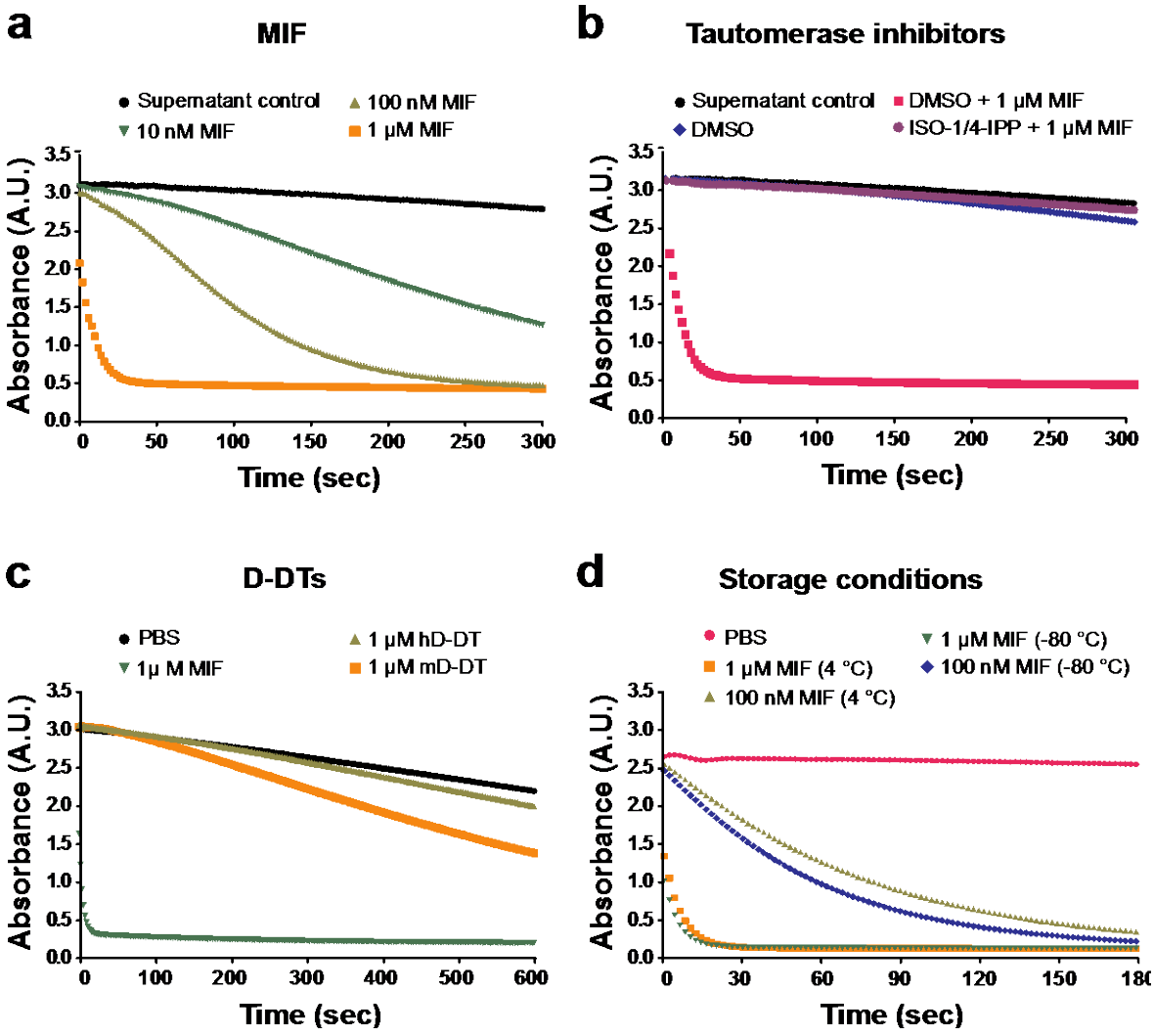

Figure S3. MIF tautomerises L-dopachrome methyl ester much faster than D-DT. Tautomerase assays were performed as described (Filip et al., 2009). Original kinetics traces of absorbance are shown over the indicated time. (**a-b**) Supernatants of COS-7/M6 cells were supplemented with increasing concentrations of MIF and stored at 37°C overnight. The next day, 400 µl of supernatant was used for the assay. The graphs represent a single replicate. (**a**) MIF tautomerises L-dopachrome methyl ester in a dose-dependent manner. MIF is stable in cell culture supernatants for at least 24 hours indicated by a negligible loss of tautomerase activity (compare a and d). (**b**) Tautomerse activity is abrogated in the

presence of 50 µM (S,R)-3-(4-hydroxyphenyl)-4,5-dihydro-5-isoxazole acetic acid (ISO-1) and 50 µM 4-iodo-6-phenylpyrimidine (4-IPP). Proteins assayed in (c-d) were diluted in PBS. (**c**) Compared to MIF, D-DT has a much lower tautomerase activity as previously described, with mouse D-DT being slightly more active than human D-DT. The graph represents triplicate values of absorbance ± standard deviation. (**d**) MIF can be stored for a prolonged time without loosing an appreciable amount of tautomerase activity. Two samples of MIF were assayed - one stored at +4 °C for a few weeks and the other one at -80 °C for more than a year before thawing. The graphs represent duplicate values of absorbance ± standard deviation.

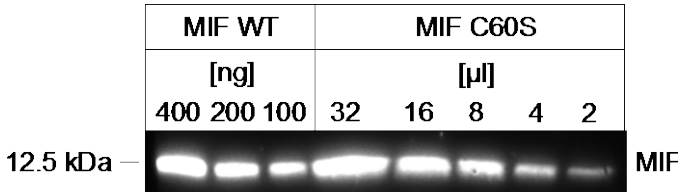

Figure S4. Aggregation prone MIF C60S mutant protein was titrated against recombinant wildtype MIF for estimating its protein concentration. MIF C60S localises to inclusion bodies during bacterial expression (Kleemann, R., Mischke, R., Kapurniotu, A., Brunner, H. and Bernhagen, J. (1998). *FEBS Lett.* 430, 191–196), and purified protein tends to precipitate after thawing. Therefore, a thawed solution of purified, concentrated MIF C60S protein was centrifuged at 16.000 g for 10 min at 4°C. The supernatant was transferred to a new microcentrifuge tube, kept at room temperature and its protein concentration measured semi-quantitatively with an immunoblot using wildtype (WT) MIF as standard (estimated as 25 ng/µl). Indicated samples were resolved by 15% SDS-PAGE and transferred to a nitrocellulose membrane. After probing with primary rabbit anti - MIF antibody and goat anti-rabbit HRP-conjugated secondary antibodies (see Table 2 for further details) protein bands were visualised with ECL. This approach ensured that the chemokinesis experiments were performed with a soluble mutant protein at the same concentration as wildtype MIF.

Primer	Sequence (5'→3')	Length [bp]	T_m [° C]	Amplicon size [bp]	Feature recognised/ Accession no.
β-actin-For	ATGGTGGGTATGGGTCAGAA	20	60.0	232	Exon 1 of AB004047.1
β-actin-Rev	GGGTCATCTTTTCACGGTTG	20	60.3		
CD74-For	ACGCTCCACCGAAAGAGTC	19	60.4	194	Spanning exon 6/7 in NM_004355.3 (For) V5 tag (Rev)
CD74-Rev	CGTAGAATCGAGACCGAGGA	20	60.3		
CD44-For	CTCCAGTGAAAGGAGCAGCA	20	60.0	146	Exon 5 (For) and Exon 6 (Rev) in NM_001001391.1
CD44-Rev	TGGGGTGGAATGTGTCTTGG	20	59.9		

Table S1. Primers used for Figure S1. (**a**) 194-bp non-intron-spanning amplicon of the transfected human CD74 sequence that is also encoding a V5 tag at the 3´-end. (**b**) 146-bp intron-spanning amplicon of the CD44 mRNA (encoding all variable v1-v10 splice variants). (**c**) An inversed and contrast-enhanced gel image of (b) is shown to better visualise low-intensity CD44 mRNA bands. (**d**) 232-bp amplicon of β-actin mRNA. (**e-g**) Cell lysates were resolved on two polyacrylamide gels, and transferred semi-dry onto nitrocellulose membranes. The membranes were probed with antibodies against (**e**) CD44 (full-length as well as truncated CD44Δ67) (Hermes-3), (**f**) CD74 (FL-296), and (**g**) β-actin and probed with HRP-conjugated secondary antibodies. Insert in (f) depicts the ECL signal with increased contrast to better visualise low levels of CD44.

Figure	COS-7/M6 cell line	Stimulation	Velocity [μm min^{-1}]		Significance
			Median	Mean ± SD (95% CI)	
Figure 1a-b	WT	NT	0.07	0.10 ± 0.09 (0.09, 0.11)	-
	WT	EGF	0.14	0.18 ± 0.14 (0.16, 0.19)	*** (vs. NT)
	WT	MIF	0.10	0.14 ± 0.11 (0.13, 0.15)	*** (vs. NT)/ * (vs. boiled MIF)
	WT	Boiled MIF	0.08	0.12 ± 0.09 (0.10, 0.13)	Ns (vs. NT)
	WT	D-DT	0.08	0.11 ± 0.09 (0.10, 0.12)	Ns (vs. NT)/ Ns (vs. boiled D-DT)
	WT	Boiled D-DT	0.07	0.10 ± 0.09 (0.09, 0.11)	Ns (vs. NT)
	WT	MIF + D-DT	0.09	0.12 ± 0.09 (0.11, 0.13)	*** (vs. NT)
	CD74$^+$/CD44$^+$	NT	0.08	0.10 ± 0.07 (0.09, 0.11)	-
	CD74$^+$/CD44$^+$	EGF	0.11	0.16 ± 0.13 (0.15, 0.18)	*** (vs. NT)
	CD74$^+$/CD44$^+$	MIF	0.11	0.14 ± 0.09 (0.13, 0.15)	*** (vs. NT)/ *** (vs. boiled MIF)
	CD74$^+$/CD44$^+$	Boiled MIF	0.08	0.10 ± 0.08 (0.09, 0.10)	Ns (vs. NT)
	CD74$^+$/CD44$^+$	D-DT	0.09	0.12 ± 0.10 (0.11, 0.13)	* (vs. NT)/ *** (vs. boiled D-DT)
	CD74$^+$/CD44$^+$	Boiled D-DT	0.07	0.09 ± 0.07 (0.08, 0.90)	** (vs. NT)
	CD74$^+$/CD44$^+$	MIF + D-DT	0.10	0.12 ± 0.10 (0.12, 0.13)	*** (vs. NT)
Figure 1c	WT	NT	0.09	0.12 ± 0.09 (0.10, 0.13)	-
	WT	MIF	0.12	0.16 ± 0.11 (0.14, 0.17)	*** (vs. NT)
	WT	MIF siRNA	0.08	0.10 ± 0.09 (0.09, 0.11)	Ns (vs. NT)
	WT	MIF siRNA + MIF	0.10	0.13 ± 0.09 (0.12, 0.14)	*** (vs. MIF siRNA)
Figure 1d	CD74$^+$/CD44$^+$	NT	0.11	0.14 ± 0.10 (0.13, 0.16)	-
	CD74$^+$/CD44$^+$	MIF	0.15	0.19 ± 0.13 (0.17, 0.21)	*** (vs. NT)
	CD74$^+$/CD44$^+$	MIF siRNA	0.09	0.11 ± 0.09 (0.10, 0.13)	** (vs. NT)
	CD74$^+$/CD44$^+$	MIF siRNA + MIF	0.11	0.14 ± 0.10 (0.13, 0.16)	*** (vs. MIF siRNA)
Figure 2a	WT	NT	0.07	0.09 ± 0.07 (0.08, 0.10)	-
	WT	MIF + EtOH	0.09	0.12 ± 0.09 (0.11, 0.13)	-
	WT	MIF	0.08	0.11 ± 0.09 (0.10, 0.12)	*** (vs. NT)
	WT	MIF + 4-IPP	0.07	0.09 ± 0.06 (0.08, 0.10)	*** (vs. MIF + EtOH)
	WT	MIF + ISO-1	0.07	0.09 ± 0.08 (0.08, 0.10)	*** (vs. MIF + EtOH)
Figure 2b	WT	NT	0.07	0.08 ± 0.06 (0.08, 0.91)	-
	WT	MIF	0.09	0.11 ± 0.06 (0.10, 0.12)	*** (vs. NT)
	WT	MIF Δ4	0.06	0.07 ± 0.05 (0.07, 0.08)	Ns (vs. NT)
	WT	MIF P2A	0.07	0.08 ± 0.04 (0.07, 0.08)	Ns (vs. NT)
Figure 2c	WT	NT	0.08	0.09 ± 0.05 (0.09, 0.10)	-
	WT	MIF	0.10	0.12 ± 0.07 (0.11, 0.13)	*** (vs. NT)
	WT	MIF C60S	0.08	0.10 ± 0.06 (0.10, 0.11)	* (vs. NT)
Figure 3a	WT	NT	0.06	0.07 ± 0.08 (0.07, 0.08)	-
	WT	MIF	0.08	0.10 ± 0.09 (0.09, 0.11)	*** (vs. NT)
	WT	CPZ	0.06	0.07 ± 0.06 (0.07, 0.08)	Ns (vs. NT)
	WT	MIF + CPZ	0.08	0.11 ± 0.09 (0.10, 0.12)	Ns (vs. CPZ)
	WT	DYN	0.05	0.06 ± 0.03 (0.05, 0.06)	** (vs. NT)
	WT	MIF + DYN	0.07	0.08 ± 0.13 (0.07, 0.10)	*** (vs. DYN)
	WT	NYS	0.05	0.06 ± 0.03 (0.06, 0.06)	Ns (vs. NT)
	WT	NYS + MIF	0.06	0.06 ± 0.03 (0.06, 0.07)	Ns (vs. NYS)
Figure 3b	CD74$^+$/CD44$^+$	NT	0.07	0.09 ± 0.06 (0.08, 0.10)	-
	CD74$^+$/CD44$^+$	MIF	0.10	0.12 ± 0.08 (0.11, 0.13)	*** (vs. NT)
	CD74$^+$/CD44$^+$	CPZ	0.08	0.11 ± 0.07 (0.10, 0.12)	** (vs. NT)
	CD74$^+$/CD44$^+$	MIF + CPZ	0.12	0.15 ± 0.10 (0.14, 0.16)	*** (vs. CPZ)
	CD74$^+$/CD44$^+$	DYN	0.07	0.07 ± 0.03 (0.07, 0.08)	* (vs. NT)
	CD74$^+$/CD44$^+$	MIF + DYN	0.07	0.08 ± 0.04 (0.07, 0.08)	*** (vs. DYN)
	CD74$^+$/CD44$^+$	NYS	0.07	0.08 ± 0.04 (0.07, 0.08)	Ns (vs. NT)
	CD74$^+$/CD44$^+$	NYS + MIF	0.07	0.09 ± 0.07 (0.08, 0.10)	Ns (vs. NYS)
Figure 3c	WT	MIF + DMSO	0.14	0.16 ± 0.10 (0.15, 0.18)	-
	WT	MIF + FIL	0.10	0.12 ± 0.07 (0.11, 0.13)	*** (vs. MIF + DMSO)
Figure 3d	CD74$^+$/CD44$^+$	MIF + DMSO	0.15	0.18 ± 0.12 (0.16, 0.19)	-
	CD74$^+$/CD44$^+$	MIF + FIL	0.12	0.13 ± 0.06 (0.12, 0.14)	*** (vs. MIF + DMSO)
Figure 3e	CD74$^+$/CD44$^+$	NT	0.11	0.13 ± 0.07 (0.12, 0.15)	-
	CD74$^+$/CD44$^+$	D-DT	0.16	0.18 ± 0.10 (0.17, 0.20)	*** (vs. NT)

Table S2. Summary of all chemokinesis results with statistical analyses. 95% CI is the lower and upper confidence interval of the mean. All treatments with recombinant proteins, tautomerase inhibitors, and ethanol were performed at 0.5% (v/v) FCS. NT = not treated i.e. 0.5% (v/v) FCS only. The treatments are statistically compared towards cognate NT controls (grouped by colour coding), and not to an overall mean of all NT values measured. Abbreviations: SD = standard deviation. Significance levels: ns, non-significant ($p > 0.05$); *, $p \leq 0.05$; **, $p \leq 0.01$; ***, $p \leq 0.001$.

Antibody	Catalogue number, manufacturer/supplier	Dilution
Anti-MIF (rabbit polyclonal)	36-7401, ThermoFisher	1:20,000
Anti-β-actin antibody (AC-15) (ascites fluid, mouse monoclonal)	A5441, Sigma-Aldrich	1:5,000
Anti-mouse CD44 (Hermes-3) (mouse mc)	Margot Zöller, Heidelberg	1:500
Purified mouse anti-human CD74 (mouse mc) (IgG2a)	555538, BD Pharmingen	1:500
Rabbit anti-CXCR4	sc-9046, Santa Cruz	1:500
Goat anti-rabbit HRP-conjugated secondary antibody	55676, MP Cappel; and 12-348, Merck	1:10,000
Sheep anti-mouse HRP-conjugated secondary antibody	A5906, Sigma-Aldrich	1:10,000

Table S3. Antibodies used for immunoblot analyses.

Name	Sequence (5’ to 3’)
ON-TARGET*plus* MIF #1	GGGUCUACAUCAACUAUUAUU
ON-TARGET*plus* MIF C911 #1	GGGUCUACUAGAACUAUUAUU
ON-TARGET*plus* MIF #2	GCGCAGAACCGCUCCUACAUU
ON-TARGET*plus* MIF C911 #2	GCGCAGAAGGCCUCCUACAUU

Table S4. siRNA sequences used to knockdown MIF. Underlined are nucleotides 9 to 11 (complementary in C911 #1 and 2 to MIF #1 and 2, respectively). C911 controls eliminate on-target effects while retaining the same off-target effects the gene-specific siRNA might have by maintaining its guide and passenger strand seed sequences (bases 2-8 and bases 12-17 respectively) (Chung et al., 2014).